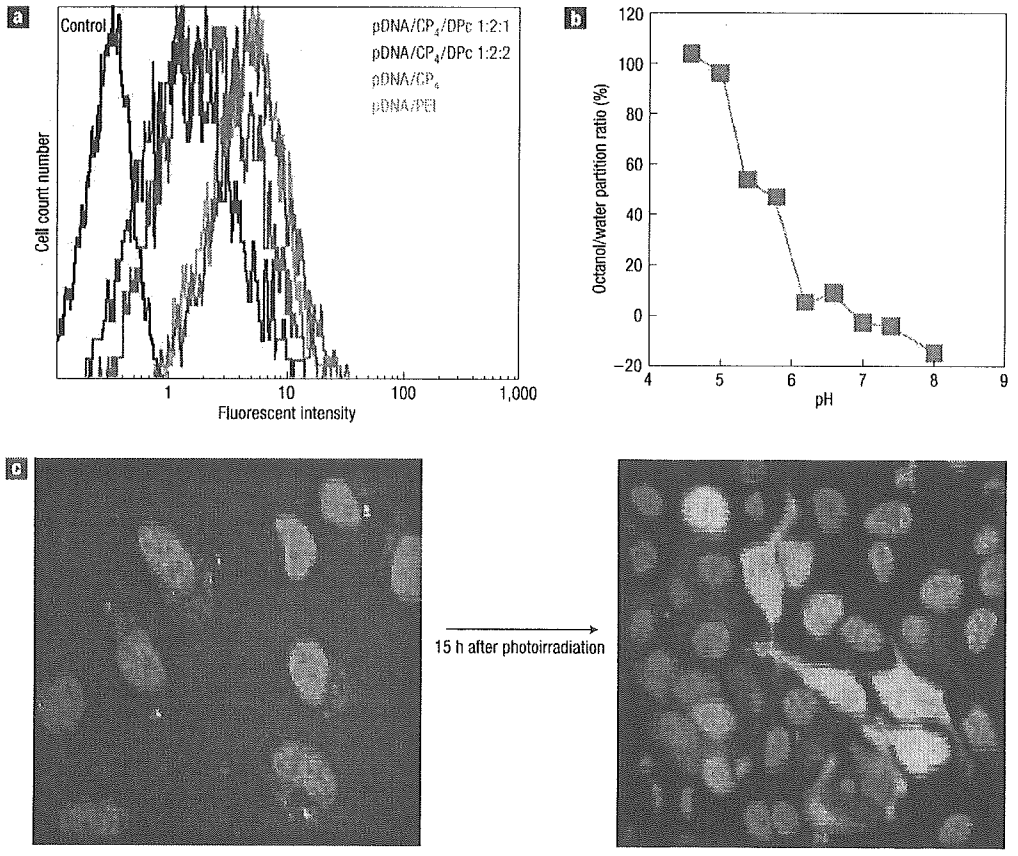

Figure 2 Properties of DPc and the pDNA/CP$_4$/DPc ternary complexes. a, Cellular uptake of the electrostatic complexes incorporating fluorescein-labelled pDNA. HeLa cells were incubated with each complex for 6 h, followed by flow cytometric analysis. The pDNA/PEI polyplex was prepared at an N/P ratio of 10. **b**, The pH-dependent partitioning (%) of DPc from the aqueous phase to the octanol phase. **c**, The intracellular distribution of FITC-dextran (green) co-incubated with the pDNA/CP$_4$/DPc complex with a charge ratio of 1:2:1 before and after photoirradiation. HeLa cells were incubated with the ternary complex for 6 h, followed by photoirradiation. The cell nuclei were stained with Hoechst 33258 (blue).

in which remarkable photochemical enhancement of the transgene expression was accomplished without compromising cell viability, ensuring the safety and effectiveness of the PCI-mediated *in vivo* gene delivery.

The reduced cytotoxicity after prolonged incubation with synthetic vectors might be one of the main criteria for successful *in vivo* transfection. In this study, the cells were photoirradiated after 6 h incubation with each complex, followed by 48-h post-incubation without medium replacement. Figure 3c shows the transfection efficiency and cytotoxicity of each complex after prolonged incubation. The 1:2:0.5, 1:2:1 and 1:2:2 ternary complexes showed 158-, 117- and 23-fold photochemical enhancement of the transfection, respectively, with approximately 20% decreases in the cell viability. In contrast, the efficient transfection by the PEI polyplex was accompanied by a remarkable decrease (~85%) in the cell viability. Thus, the PCI-mediated gene delivery can avoid long-term toxicity, which is often induced by the polyplexes based on buffering polycations, because the process toxic to the cell is controlled in a light-responsive manner. Also, the ternary complex with a negative ζ-potential value might hardly interact with the negatively charged cell membranes, leading to reduced cytotoxicity in long-term incubation.

The potential of the ternary complex for *in vivo* PCI-mediated gene delivery was studied by the transfection of a reporter gene (a variant of yellow fluorescent proteins, Venus) to the conjunctival tissue in rat eyes on laser irradiation. In this study, the rat eyes received a subconjunctival injection of the ternary complex (360° circumferential to the cornea), and part of the conjunctiva was then irradiated with a semiconductor laser (689 nm) at 2 h post-injection (Fig. 4a). The pDNA/CP$_4$/DPc ternary complex with a charge ratio of 1:2:1 achieved significant gene expression only at the laser-irradiated site in the conjunctiva in 8 out of 12 eyes (2 days after irradiation; Fig. 4b,c). Neither the ternary complexes with different compositions (that is, the 1:2:0.5 and 1:2:2 ternary complexes) nor ExGen500, which is one of the most efficient synthetic vectors, showed visible transgene expression. With the passage of time, the number of transfected eyes as well as the fluorescent intensity significantly decreased (Fig. 4c). Fluorescent microscopic observation of a frozen section of the conjunctival tissue revealed that the conjunctival epithelial cells were clearly transfected (Fig. 4d,e). Thus, the transfection only at the laser-irradiated site in the conjunctival tissue was achieved by the PCI-mediated gene delivery using the ternary complex. To our knowledge, this is the first success in PCI-mediated gene delivery *in vivo*.

PCI is a smart concept, which allows the cytoplasmic delivery of macromolecular compounds in a light-inducible

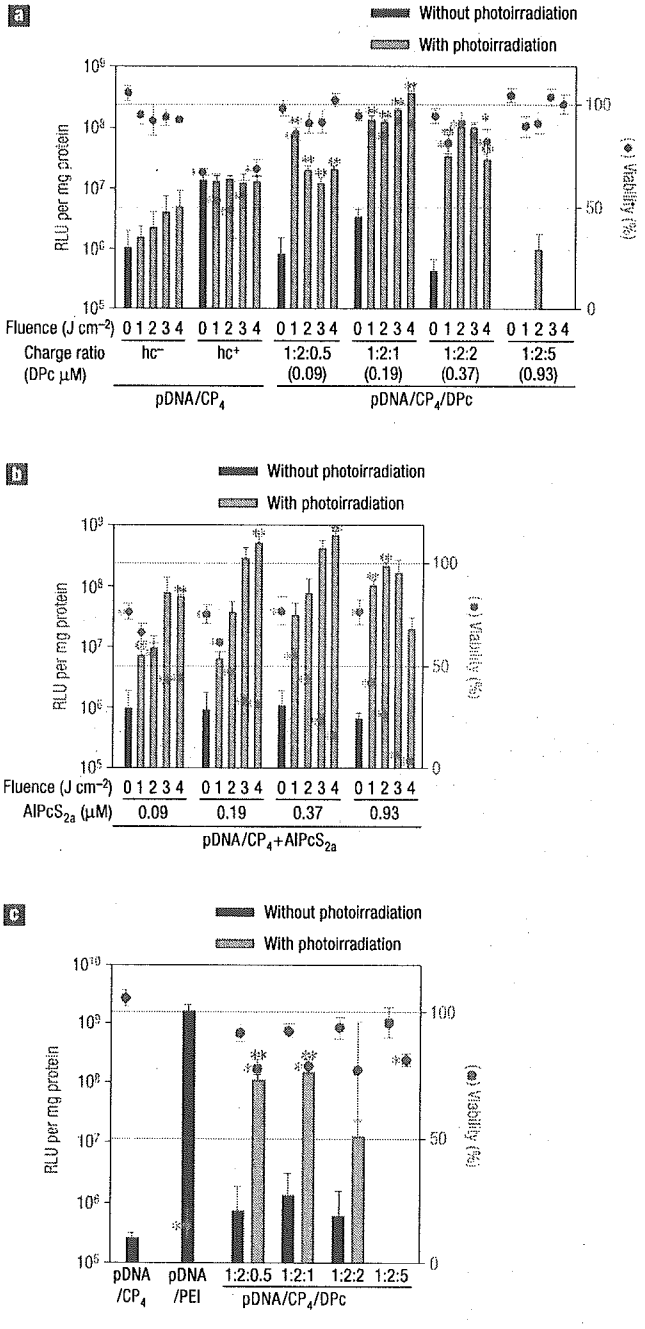

Figure 3 *In vitro* tranfection efficiency and cytotoxicity to HeLa cells. a, The effect of fluence on the transfection efficiency (bars) and photocytotoxicity (dots) of the pDNA/CP_4 and pDNA/CP_4/DPc complexes. Photoirradiation was performed 6 h after incubation with each complex, followed by 48 h post-incubation in a fresh medium. The hc represents hydroxychloroquine. **b**, The effect of fluence on the transfection efficiency (bars) and photocytotoxicity (dots) of the pDNA/CP_4 complex with different concentrations of $AlPcS_{2a}$. The same experimental conditions as **a** were applied. **c**, The transfection efficiency (bars) and photocytotoxicity (dots) when HeLa cells were irradiated 6 h after incubation with each complex at 3.6 J cm^{-2}, followed by 48 h post-incubation without medium replacement. Results are expressed as mean ± s.d. ($n = 4$). The unpaired t-test was used for statistical analysis, and significant changes in the cell viability (treated to untreated) and the transfection efficiency (photoirradiated to non-photoirradiated) are indicated by asterisks * and **, respectively.

manner. In previous studies, it was demonstrated that $AlPcS_{2a}$ and $TPPS_{2a}$ (meso-tetraphenylporphine with two sulphonate groups on adjacent phenyl rings) were effective in PCI-mediated delivery[8–10]. It is assumed that a hydrophobic moiety in these dissymmetric compounds may provide preferable interaction with cell membranes, whereas they are internalized by endocytosis because of high water solubility. However, such an amphiphilic nature of the compounds should generate interaction with the plasma membrane to some extent, possibly photodamaging the plasma membrane. Meanwhile, such amphiphilic photosensitizers may relocalize to some cytoplasmic organelles such as mitochondria and endoplasmic reticulum during the photoirradiation[11,22,23]. It is known that the plasma membrane and some cytoplasmic organelles might be susceptible to the photocytotoxicity[11]. These effects may be a major cause of the photocytotoxicity of $AlPcS_{2a}$ and $TPPS_{2a}$. These compounds are still useful in PCI; however, reduced photocytotoxicity might be desired before considering further applications of this technology. We assume that the selective photodamage of the endosomal membrane is a key to reduced photocytotoxicity in PCI, motivating us to develop different gene carriers based on the PCI concept.

To design gene carriers based on the PCI concept, the following points should be considered. (i) For *in vivo* applications, the photosensitizing units should be integrated into gene carriers as one component, because separate administration of photosensitizers might result in their diffused localization to the surrounding tissues, which may decrease the efficiency in the PCI-mediated gene delivery and cause the phototoxicity to the surrounding tissues. (ii) Following internalization by the endocytosis, the photosensitizers should be released from gene carriers, otherwise, pDNA could be photochemically inactivated on photoirradiation. (iii) The photosensitizers should have increased affinity for cell membranes under endosomal conditions to accomplish the photochemical rupture of the endosomal membrane. In the ternary complex system, we suggest that DPc may be released from the complex to interact with the endosomal membrane (Fig. 2b), satisfying the aforementioned requirements for effective PCI-mediated gene delivery (Fig. 5).

In *in vitro* experiments, both the ternary complex and the PCI using $AlPcS_{2a}$ showed reduced cell viability as the fluence increased, and the degree of the cytotoxicity depended on the cell lines (Fig. 3a,b, and see Supplementary Information, Figs S1 and S2). Indeed, the PCI conditions have been optimized depending on each cell line[9,10]. However, in this study, a comparison under the same experimental conditions revealed that the ternary complex showed a wider range of safe light doses, in which remarkable enhancement of the transfection was accomplished without reduced cell viability, irrespective of cell lines and incubation time (Fig. 3a and see Supplementary Information, Fig. S2). These results may be due to control of the initial steps in the PCI and highly selective photodamage to the endosomal membrane as described above. We believe that such an expanded range of safe light dose might have resulted in our success in the PCI-mediated gene delivery *in vivo*.

The reduced photocytotoxicity of the ternary complexes might be one of the most important achievements in this study. Because of the pH-dependent membrane binding ability of DPc (Fig. 2b), the photocytotoxicity seems to be reduced when DPc is relocated from the acidic endocytic vesicles into the cytosol. A cytosolic localization of DPc may not be expected to cause phototoxicity owing to low stability of singlet oxygen in aqueous media. Alternatively, it seems that DPc may undergo slower diffusion in the cytosol because of its larger size compared with $AlPcS_{2a}$ and have a reduced chance of relocalizing in susceptible cytoplasmic organelles. However, these assumptions remain to be clarified.

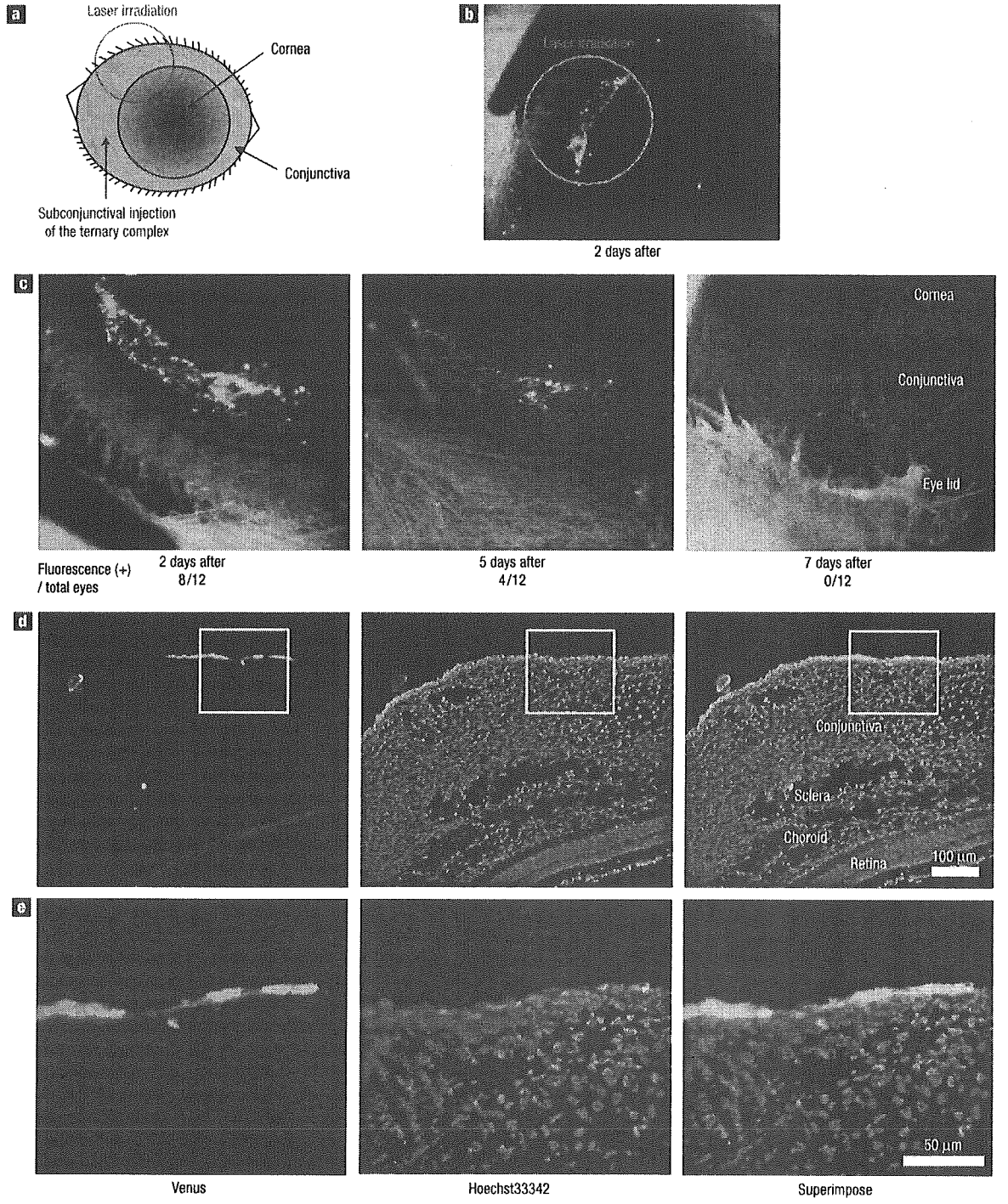

Figure 4 Transfection to the conjunctival tissue to rat eyes. a, The scheme for *in vivo* transfection. Rats were given a subconjunctival injection (coloured in light blue) of each complex containing 15 μg pDNA encoding a variant of a yellow fluorescent protein (Venus). At 2 h post-injection, a part of the conjunctiva (red circle) was irradiated with a light of 689 nm. **b,c**, Fluorescent images of the Venus expression in the rat eye at 2, 5 and 7 days after the photochemical transfection using the 1:2:1 ternary complex. The fluorescent-positive eyes/total eyes are indicated below the images. **d**, A fluorescent image of the Venus expression in the frozen section of the conjunctival tissue. The image was taken 2 days after the photochemical transfection using the pDNA/CP_4/DPc 1:2:1 ternary complex. The cell nuclei were stained in blue. **e**, A magnified image of the white square in the above fluorescent image.

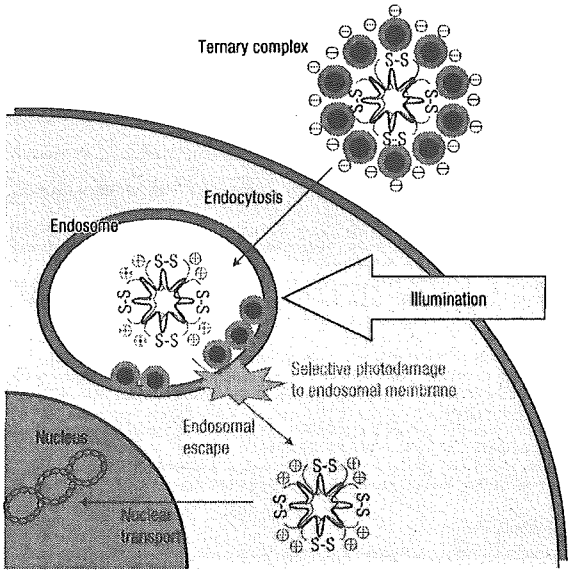

Figure 5 A scheme for itinerary of the ternary complex to the transgene expression. The ternary complex was designed to control the initial steps (that is, internalization by the endocytosis and photodamage of the endosomal membrane to release the polyplex to the cytoplasm) in the PCI-mediated gene delivery.

In the ternary complex system, there is still room for optimization of each component. For example, the polyplex-forming polycations can be optimized, because a variety of polycations can be used for the formation of the ternary complex. Indeed, the ternary complex was formed from poly(L-lysine) at a charge ratio of 1:2:2 (see Supplementary Information, Table S1), and the pDNA/poly(L-lysine)/DPc ternary complex showed approximately 15-fold photochemical enhancement of the transfection with a 50% decrease in the cell viability (see Supplementary Information, Fig. S3). This result suggests that the polyplex-forming polycations significantly affect the transfection efficiency and cytotoxicity, highlighting the importance of optimization of the polycations. In the present study, the CP_4 peptide, of which the nuclear localization and the effective gene transfection following the translocation into the cytoplasm were demonstrated in the previous study[17], was used to prepare the ternary complex, and we successfully obtained the PCI-mediated gene transfection *in vitro* and *in vivo*. Further optimization of the polycations is our future interest, and the studies in this direction will be reported elsewhere.

This system can be potentially useful for the gene therapy of ophthalmic diseases[24]. The molecular design could be expanded to a systemically targeted gene carrier for the treatment of various diseases, including solid tumours. Spatial control of transgene expression in the body will ensure the effectiveness and safety of *in vivo* gene therapy.

METHODS

POLYMER SYNTHESIS AND CHARACTERIZATION

Synthesis of ionic DPc (Fig. 1a) was performed according to the method reported in ref. 25. The detailed synthetic procedure is described in Supplementary Information. The absorption spectra revealed that DPc shows B band absorption at 350 nm and strong Q band absorption at 685 nm.
A cationic peptide $C(YGRKKRRQRRRG)_2$ (CP_2) was synthesized by the Peptide Institute (Osaka, Japan). The CP_4 peptide was prepared by oxidation of the CP_2 peptide in 10 mM of Tris–HCl buffer (pH 7.4) over 14 days. PAA homopolymer (DP: 26; weight-averaged/number-averaged molecular mass (M_w/M_n), 1.2) was synthesized as reported in ref. 26.

PLASMID DNA

A plasmid DNA, pCAcc+Luc, containing a firefly luciferase cDNA driven by a CAG promoter[27] was provided by RIKEN Bioresource Centre (Tsukuba, Japan). Also, a fragment cDNA of SEYFP-F46L (Venus), which is a variant of a yellow fluorescent protein with the mutation F46L[28], was provided by A. Miyawaki of the Brain Science Institute, RIKEN (Wako, Japan), and inserted into the pCAcc vector (pCAcc+Venus). Each plasmid DNA (pDNA) was amplified in competent DH5α *Escherichia coli* and purified by a HiSpeed Plasmid Maxi Kit (Qiagen, Germany). pCAcc+Luc was used for *in vitro* studies, whereas *in vivo* transfection was performed using pCAcc+Venus.

PREPARATION OF THE TERNARY COMPLEX

The pDNA/CP_4 polyplex was prepared by mixing pDNA and CP_4 peptide in 10 mM of Tris–HCl buffer (pH 7.4) at an N/P ratio of 2 (pDNA concentration, 100 μg ml^{-1}). At 30 min after incubation at ambient temperature, the pDNA/CP_4 polyplex solution was mixed with the DPc solution with varying charge molar ratios of pDNA/CP_4/DPc, followed by an extra 30-min incubation at ambient temperature to obtain the pDNA/CP_4/DPc ternary complex. The ternary complexes with varying ratios of DPc were characterized by a gel retardation assay.

CHARACTERIZATION OF THE TERNARY COMPLEX

The size and polydispersity were evaluated by dynamic light scattering measurements using a DLS-7000 instrument (Otsuka Electronics, Osaka, Japan) equipped with an Ar-ion laser (488 nm). The ζ-potential was measured by a laser-Doppler electrophoresis ELS-6000 instrument (Otsuka Electronics) equipped with a He–Ne ion laser (633 nm). AFM imaging was performed in a tapping mode with a standard silicon probe 160 μm in length using an NVB 100 microscope (Olympus, Tokyo, Japan) operated by Nanoscope IIIa software (Digital Instruments, Santa Barbara, California). Detailed experimental conditions are described in the Supplementary Information.

OCTANOL/WATER PARTITIONING

The experimental procedure is described in the Supplementary Information.

FLOW CYTOMETRY ANALYSIS AND CONFOCAL MICROSCOPIC OBSERVATION

The amount of uptake of each polyplex containing pDNA labelled with fluorescein by HeLa cells was analysed by flow cytometry. The detailed experimental conditions are described in the Supplementary Information. Confocal observation of FITC-labelled dextran (M_w: 10,000–15,000) co-incubated with the 1:2:1 ternary complex in HeLa cells before and after photoirradiation was performed using LSM510 (Carl Zeiss, Jena, Germany). Detailed experimental conditions are provided in the Supplementary Information.

IN VITRO TRANSFECTION STUDY

HeLa cells (10,000 cells) on a 24-well culture plate were incubated with each polyplex containing 1 μg pDNA in 0.5 ml of Dulbecco's Modified Eagle's Medium (DMEM) containing 10% fetal bovine serum (FBS), followed by 6- or 24-h incubation and fresh medium replacement. The culture plates were photoirradiated using a 300-W halogen lamp (fluence rate, 3.0 mW cm^{-2}) equipped with a band-pass filter (400–700 nm) with increased fluence (0.9–3.6 J cm^{-2}). After 48 h post-incubation, the transfection efficiency was evaluated by the Luciferase Assay System (Promega, Madison, Wisconsin) and a Lumat LB9507 luminometer (Berthold Technologies, Bad Wildbad, Germany), whereas the cell viability was evaluated by the 3-(4,5-dimethylthiazol-2-yl)-2,5-diphenyltetrazolium bromide (MTT) assay. Sulphonated aluminium phthalocyanine ($AlPcS_{2a}$) and PEI (25 kDa) were purchased from Frontier Scientific (Logan, Utah) and Sigma-Aldrich (St Louis, Missouri), respectively.

IN VIVO TRANSFECTION TO CONJUNCTIVA

Wistar rats (male, 6 weeks old, number of animals $n = 12$; Saitama Experimental Animal Supply, Saitama, Japan) were given a subconjunctival injection of 150 μl of each complex containing 15 μg pDNA (pCAcc+Venus). At 2 h post-injection, the rats were anesthetized and part of the conjunctiva was irradiated using a 689-nm semiconductor laser emitted from laser equipment built in-house (Topcon, Tokyo, Japan) with 2.0 mW laser power and 4 mm projection diameter for 60 s (1 J cm^{-2}). The fluorescent images of the Venus

expression in a rat eye and the conjunctival tissues were taken as described in Supplementary Information. All the experimental procedures were handled in accordance with the guidelines of the Animal Committee of the University of Tokyo. The polyplex from linear PEI, with ExGen500 (Fermentas, Vilnius, Lithuania) as a control vector, was prepared at N/P ratio = 6.

Received 12 July 2005; accepted 28 September 2005; published 20 November 2005.

References

1. Ogris, M. & Wagner, E. Targeting tumors with non-viral gene delivery systems. *Drug Discov. Today* **7**, 479–485 (2002).
2. Taira, K., Kataoka, K. & Niidome, T. (eds) *Non-viral Gene Therapy: Gene Design and Delivery* (Springer, Tokyo, 2005).
3. Merdan, T., Kopecek, J. & Kissel, T. Prospects for cationic polymers in gene and oligonucleotide therapy against cancer. *Adv. Drug Deliv. Rev.* **54**, 715–758 (2002).
4. Salem, A. K., Searson, P. C. & Leong, K. W. Multifunctional nanorods for gene delivery. *Nature Mater.* **2**, 668–671 (2003).
5. Behr, J. P. The proton sponge. A trick to enter cells the viruses did not exploit. *Chimia* **51**, 34–36 (1997).
6. Berg, K. *et al.* Photochemical internalization: a novel technology for delivery of macromolecules into cytosol. *Cancer Res.* **59**, 1180–1183 (1999).
7. Høgest, A., Prasmickaite, L., Tjelle, T. E. & Berg, K. Photochemical transfection: A new technology for light-induced, site-directed gene delivery. *Hum. Gene Ther.* **11**, 869–880 (2000).
8. Prasmickaite, L., Høgest, A. & Berg, K. Evaluation of different photosensitizers for use in photochemical gene transfection. *Photochem. Photobiol.* **73**, 388–395 (2001).
9. Høgest, A. *et al.* Photochemical transfection: A technology for efficient light-directed gene delivery. *Somat. Cell Mol. Genet.* **27**, 97–113 (2002).
10. Høgest, A. *et al.* Photochemical internalization in drug and gene delivery. *Adv. Drug Deliv. Rev.* **56**, 95–115 (2004).
11. Macdonald, I. J. & Dougherty, T. J. Basic principle of photodynamic therapy. *J. Porphyrins Phthalocynanines* **5**, 105–129 (2001).
12. Esfand, R. & Tomalia, D. A. Poly(amidoamine) (PAMAM) dendrimers: from biomimicry to drug delivery and biomedical applications. *Drug Discov. Today* **6**, 427–436 (2001).
13. Gillies, E. R. & Frechet, J. M. Dendrimers and dendritic polymers in drug delivery. *Drug Discov. Today* **10**, 35–43 (2005).
14. Duncan, R. The dawning era of polymer therapeutics. *Nature Rev. Drug Discov.* **2**, 347–360 (2003).
15. Kobayashi, H. *et al.* Lymphatic drainage imaging of breast cancer in mice by micro-magnetic resonance lymphangiography using a nano-size paramagnetic contrast agent. *J. Natl Cancer Inst.* **96**, 703–708 (2004).
16. Tang, M., Redemann, C. T. & Szoka, F. C. Jr. In vitro gene delivery by degraded polyamidoamine dendrimers. *Bioconjugate Chem.* **7**, 703–714 (1996).
17. Rudolph, C. *et al.* Oligomers of the arginine-rich motif of the HIV-1 TAT protein are capable of transferring plasmid DNA into cells. *J. Biol. Chem.* **278**, 11411–11418 (2003).
18. Caruso, F., Caruso, R. A. & Möhwald, H. Nanoengineering of inorganic and hybrid hollow spheres by colloidal templating. *Science* **282**, 1111–1114 (1998).
19. Donath, E. *et al.* Novel hollow polymer shells by collid-templated assembly of polyelectrolytes. *Angew. Chem. Int. Edn* **37**, 2002–2005 (1998).
20. Levitan, H. & Barker, J. L. Salicylate. Structure-activity study of its effects on membrane permeability. *Science* **176**, 1423–1425 (1972).
21. Itaka, K. *et al.* in *Carrier-Based Drug Delivery* (ed. Svenson, S.) 154–159 (ACS Symp. Series Vol. 879, Americal Chemical Society, 2004).
22. Moan, J., Berg, K., Anholt, A. & Madslien, K. Sulfonated aluminum phthalocyanines as sensitizers for photochemotherapy. Effects of small doses on localization, dye fluorescence and photosensitivity in V79 cells. *Int. J. Cancer* **58**, 865–870 (1994).
23. Rodal, G. H., Rodal, S. K., Moan, J. & Berg, K. Liposome-bound Zn(II)-phthalocyanine. Mechanisms for cellular uptake and photosensitization. *J. Photochem. Photobiol. B* **45**, 150–159 (1998).
24. Daiger, S. P. Was the human genome project worth the efforts? *Science* **308**, 362–364 (2005).
25. Ng, A. C. H., Li, X. & Ng, D. K. P. Synthesis and photophysical properties of nonaggregated phthalocyanines bearing dendritic substitutes. *Macromolecules* **32**, 5292–5298 (1999).
26. Harada, A. & Kataoka, K. Formation of polyion complex micelles in aqueous milieu from a pair of oppositely-charged block copolymers with poly(ethylene glycol) segments. *Macromolecules* **28**, 5294–5299 (1995).
27. Niwa, H., Yamamura, K. & Miyazaki, J. Efficient selection for high-expression transfectants with a novel eukaryotic vector. *Gene* **108**, 193–199 (1991).
28. Nagai, T. *et al.* A variant of yellow fluorescent protein with fast and efficient mutation for cell-biological applications. *Nature Biotechnol.* **20**, 87–90 (2002).

Acknowledgements

We thank N. Kanayama (the University of Tokyo), S. Kawauchi (National Defense Medical College) and K. Date (the University of Tokyo) for technical assistance. This work was supported in part by the Core Research Program for Evolutional Science and Technology (CREST) from Japan Science and Technology Agency (JST).

Correspondence and requests for materials should be addressed to K.K.[1]

Supplementary Information accompanies this paper on www.nature.com/naturematerials.

Competing financial interests

The authors declare that they have no competing financial interests.

Available online at www.sciencedirect.com
SCIENCE DIRECT®
Polymer 46 (2005) 7749–7758
polymer
www.elsevier.com/locate/polymer

Characterization of stable lysozyme-entrapped polyion complex (PIC) micelles with crosslinked core by glutaraldehyde

Xiaofei Yuan[a], Yuichi Yamasaki[a], Atsushi Harada[b], Kazunori Kataoka[a,c,*]

[a]*Department of Materials Engineering, Graduate School of Engineering, The University of Tokyo, 7-3-1 Hongo, Bunkyo-ku, Tokyo 113 8656, Japan*
[b]*Department of Applied Materials Science, Graduate School of Engineering, Osaka Prefecture University, 1-1 Gakuen-cho, Sakai, Osaka 599 8531, Japan*
[c]*Center for Disease Biology and Integrative Medicine, Graduate School of Medicine, The University of Tokyo, 7-3-1 Hongo, Bunkyo-ku, Tokyo 113-0033, Japan*

Received 21 December 2004; accepted 16 February 2005
Available online 23 May 2005

Abstract

To gain an insight into the effect of core-crosslinking on polyion complex (PIC) micelles, the properties of PIC micelles prepared by mixing model protein, chicken egg white lysozyme with the synthesized α-methoxy-poly(ethylene glycol)–poly(α,β-aspartic acid) block copolymer (PEG–P(Asp)–NH_2) followed by glutaraldehyde addition, were investigated in detail. The added glutaraldehyde interacted with both of the lysine residues in lysozyme and P(Asp) ω-end amino groups in the micellar core, which elicited variations in the spectroscopic characteristics of the entrapped lysozyme, but no changes in its secondary structure. Micellar tolerability versus dilution, ionic strength increase, organic agent addition, and pH variation were all notably improved possibly due to strong core–shell structure-fixation resulting from this crosslinking. Such crosslinking may inhibit lysozyme denature in the presence of an organic agent, and also may prevent lysozyme escape from the micellar core usually observed due to weak association force between the lysozyme and P(Asp) segments. Additionally, the lysozyme reactivity in the micelles before and after the crosslinking seemed identical and even higher than that for free lysozyme. Such obtained stable protein-entrapped PIC micelles may find new applications in the fields of biotechnology and pharmaceutical sciences as a novel bioconjugating system.

Keywords: Polyion complex (PIC) micelles; Poly(ethylene glycol)–poly(α,β-aspartic acid) block copolymer; Lysozyme

1. Introduction

Taking advantage of advanced biotechnologies [1,2], and considering the increased awareness about bioactivities of various proteins, the therapeutic utilities of proteins as biopharmaceutical agents present more and more promising prospects. However, proteins are inherently both physically and chemically unstable [3], and biopharmaceutical utilities attempt to promote their stabilization. It has been noted that a matrix-encapsulation method may overcome this obstacle, and now the most widely studied protein encapsulating system, particularly useful in biomedical field, is based on the use of biodegradable polymer matrices, such as poly(lactide-*co*-glycolide) [4]. Nevertheless, such method requires complicated formulation procedures and the use of toxic organic solvents, both of which may perturb the protein structure and thus induce decreased bioactivities [5].

Our research group has recently established a very simple but appreciably stable protein nano-encapsulation system [6]: the core-crosslinked polyion complex (PIC) micelles, obtained by glutaraldehyde (a mild crosslinking agent for protein immobilization [7]) addition after the association of α-methoxy-poly(ethylene glycol)–poly(α,β-aspartic acid) block copolymer (PEG–P(Asp)–NH_2) as a block aniomer with a model cationic protein, trypsin. Higher apparent micellar enzymatic reactivity than free trypsin was observed because of the improved micellar stability together with the diminished trypsin self-digestion (autolysis). This system can be regarded as a novel bio-nanoreactor potentially useful in the bioengineering field.

* Corresponding author. Address: Department of Materials Engineering, Graduate School of Engineering, The University of Tokyo, 7-3-1 Hongo, Bunkyo-ku, Tokyo 113-8656, Japan. Tel.: +81 3 5841 7138; fax: +81 3 5841 7139.
E-mail address: kataoka@bmw.t.u-tokyo.ac.jp (K. Kataoka).

0032-3861/$ - see front matter © 2005 Elsevier Ltd. All rights reserved.
doi:10.1016/j.polymer.2005.02.121

To get more detailed insight into the structure and the functions of this stabilized nanoreactor system containing an enzyme, thorough investigations were performed in this study on this type of core-crosslinked PIC micelles, prepared through electrostatic interactions between PEG–P(Asp)–NH_2 block copolymer with an cationic enzyme, chicken egg-white lysozyme. Characteristics for the micelles before crosslinking have been well specified by our group [8]. The variations in entrapped lysozyme conformations, ultraviolet absorption as well as fluorescence emission spectra, and apparent enzymatic reactivity were evaluated here in detail in relation to the core-crosslinking structure of PIC micelles.

2. Experimental section

2.1. Materials

α-Methoxy-poly(ethylene glycol)–poly(α,β-aspartic acid) (PEG–P(Asp)–NH_2, M_w of PEG: 12,000, degree of polymerization (DP) of (P(Asp): 34) and α-methoxy-poly(ethylene glycol)–poly(β-benzyl-L-aspartate) (PEG–PBLA–NH_2, M_w of PEG: 12,000, DP of PBLA: 36) block copolymers, were separately synthesized as previously reported [9]. Glutaraldehyde (25% aq. solution) and chicken egg-white lysozyme were obtained from Sigma (St Louis, MO, USA). 2,4,6-Trinitrobenzenesulfonic acid sodium salt dihydrate (TNBS), N^{α}-acetyl-L-lysine methyl ester hydrochloride (Ac-lysine-OMe·HCl), pyridinium chloride, and dioxane were purchased from Wako Pure Chemical Industries, Ltd (Osaka, Japan). *p*-Nitrophenol was purchased from ICN MP Biomedicals Inc. (Irvine, CA, USA). *p*-Nitrophenyl tetra-*N*-acetyl-β-chitotetraoside (NP-$(GlcNAc)_4$) used as a synthesized substrate for lysozyme was provided by Seikagakukogyo Co. Ltd (Osaka, Japan). These reagents were used without further purification.

2.2. Synthesis of PEG–P(Asp)–NH–$COCH_3$ block copolymer

α-Methoxy-ω-acetyl-poly(ethylene glycol)–poly(α,β-aspartic acid) block copolymer (PEG–P(Asp)–NH–$COCH_3$) was obtained by eliminating the β-benzyl groups in the side chain of α-methoxy-ω-acetyl-poly(ethylene glycol)–poly(β-benzyl-L-aspartate) block copolymer (PEG–PBLA–NH–$COCH_3$) using alkali hydrolysis method [9]. This PEG–PBLA–NH–$COCH_3$ was prepared by ω-end acetylation of PEG–PBLA–NH_2, which was carried out in anhydrous DMF solvent at 40 °C for 2 h using acetic anhydride as acetylation reagent [6]. ^{1}H NMR measurement (270 MHz) was performed at 80 °C for the PEG–PBLA–NH–$COCH_3$ in DMSO-d_6 to determine the acetylation degree of the terminal primary amino groups that was found to be 90% by calculating the peak intensity ratio of the introduced acetyl protons ($COCH_3$: $\delta = 1.8$ ppm) to the PEG methylene protons (OCH_2CH_2: $\delta = 3.7$ ppm).

2.3. Formulation of crosslinked PIC micelles

The PEG–P(Asp)–NH_2 or PEG–P(Asp)–NH–$COCH_3$ block copolymer, and chicken egg white lysozyme were separately dissolved in a phosphate buffer (PBS, 10 mM, pH 7.4; $Na_2HPO_4 \cdot 12H_2O$: 2.865 g/L, $NaH_2PO_4 \cdot 2H_2O$: 0.312 g/L). After a filtration through a 0.1 μm filter to remove any dust, the block copolymer solution was mixed with the lysozyme solution to form PIC micelle followed by incubation at 25 °C over 24 h. The mixing ratio (r) of Asp residues in the P(Asp) segments to Lys and Arg residues in the lysozyme was set as unity. A given amount of glutaraldehyde (5.1 μL) was added into the PIC micelle solution (10 mL, total concentration = 1.0 mg/mL) to crosslink the micellar core through a reaction with the lysine residues on the surface of lysozyme for 30 h at 25 °C. By a dialysis against PBS to remove excess glutaraldehyde using a semi-permeable regenerated cellulose membrane with a molecular weight cut off (MWCO) = 3500, core-crosslinked PIC micelles was obtained after a further incubation at 25 °C over 24 h. Such obtained micelles was abbreviated as g-GR, where GR stands for the ratio of [aldehyde groups in glutaraldehyde] to [Lys residues in lysozyme] in the reaction mixture.

2.4. Free amino group content

Un-crosslinked lysine residues in the micellar core, expressed as the number of free amino groups per lysozyme molecule (N_{lysine}), were determined using TNBS [10a]. Briefly, a micelle solution and PBS (control solution) in identical volume were separately mixed and reacted with a given amount of TNBS solution (around 51-fold excess per lysine residue [10b]) in a dark place at 25 °C. The product of this reaction gives an absorbance around 340 nm after mixing with 10 w/v% sodium lauryl sulfate (SDS) solution and 0.2 M HCl [10a,c]. Therefore, the reacted lysine residues with TNBS was calculated from the difference in the absorption between the micelle and control PBS solutions. The molar absorption coefficient at 340 nm, $\Delta\varepsilon_{340}$, was estimated from the same procedure using Ac-lysine-OMe·HCl as a model of lysine residues, and was calculated to be 1.32×10^4 M^{-1}/cm, which is consistent with the reported values [10c].

2.5. Light scattering measurements

Light scattering measurements were carried out using a DLS-7000 instrument (Otsuka Electronic Co., Ltd, Japan). Vertically polarized light of 488 nm wavelength from an Ar ion laser (75 mW) was used as the incident beam.

In the dynamic light scattering (DLS) measurement, the photoelectron-count time correlation function, $g(\tau)$, was

analyzed using the cumulant method. It is expressed by the following equation:

$$g(\tau) = \exp[-\bar{\Gamma}\tau + (\mu_2/2)\tau^2 - (\mu_3/3!)\tau^3 \cdots] \quad (1)$$

where τ is the delay time, and $\bar{\Gamma}$ is the average characteristic line width. This equation yields a variance, $\mu_2/\bar{\Gamma}^2$, called the polydispersity index (PDI). From the $\bar{\Gamma}$, the z-averaged diffusion coefficient, D, furthermore the corresponding hydrodynamic radius, R_h, can then be calculated using the following equations:

$$\bar{\Gamma} = Dq^2 \quad (2)$$

$$q = (4\pi n/\lambda)\sin(\theta/2) \quad (3)$$

$$R_h = \frac{k_B T}{(6\pi\eta D)} \quad (4)$$

Here q is the magnitude of the scattering vector, θ is the detection angle, k_B is the Boltzmann constant, T is the absolute temperature, and η is the solvent viscosity. The size distribution was estimated from the correlation function profile using the histogram method [11].

In the static light scattering (SLS) measurement, the light scattered by a dilute polymer solution at $\theta = 0$ that obtained by extrapolation is expressed as the following equations:

$$\frac{KC}{\Delta R_0} \approx \frac{1}{M_{w,app}} + 2A_2C \quad (5)$$

$$K = \frac{(4\pi^2 n^2 (dn/dc)^2)}{(N_A \lambda^4)} \quad (6)$$

where C is the polymer concentration, ΔR_0 is the difference of the Rayleigh ratio between the solution and the solvent, $M_{w,app}$ is the apparent weight average molar mass, A_2 is the second virial coefficient, dn/dc is the refractive index increment, and N_A is the Avogadro's number.

2.6. Spectroscopic measurements

Circular dichroism (CD) spectra were measured at two wavelength regions of 200–240 nm and 260–310 nm with a J-720W spectropolarimeter (Jasco, Tokyo, Japan) using a 0.1 cm quartz cell at 25 °C. All data were expressed as molar ellipticity $[\theta]$.

Fluorescence emission spectra were obtained upon excitation at 293 nm and measured with a PF-6500 spectrofluorometer (Jasco) using a 0.1 cm quartz cell at 25 °C.

The turbidity variations in lysozyme solution (1.0 mg/mL) with 40 or 50 v/v% of dioxane were monitored at 25 °C for 30 min at a wavelength of 500 nm using a V-550 spectrophotometer (Jasco). Ultraviolet (UV) absorption spectra were also obtained using the same instrument. Unless otherwise noted, all measurements in this study were performed at 25 °C.

2.7. Apparent enzymatic activity

Free lysozyme, un-crosslinked and crosslinked micelles with identical lysozyme concentration (=4.0 mg/mL; 0.14 μmol/mL), were separately reacted with NP-$(GlcNAc)_4$ stock solution at 25 °C. By monitoring the released amount of p-nitrophenol at 400 nm using the spectrophotometer V-550, apparent reactive velocity, v_{app}, of this reaction was determined. The NP-$(GlcNAc)_4$ concentration was adjusted to 37.5 μM in the mixtures. Extinction coefficient for the p-nitrophenol at 400 nm was calculated to be $1.14 \times 10^4\ M^{-1}$/cm from the calibration curve of p-nitrophenol phosphate solution at pH = 7.4.

3. Results and discussion

3.1. Suitable GR values for crosslinked PIC micelles

The DLS and SLS measurements were performed for the PIC micelles that reacted with glutaraldehyde at GR ratios (=[aldehyde groups in glutaraldehyde]/[Lys residues in lysozyme]) of 0, 2, 4, 10, and 50, respectively, in order to monitor the variations in micellar size and light scattering intensity resulting from the core-crosslinking. As seen in Fig. 1, similar GR value dependences were observed for cumulant diameter (d_c) and light scattering intensity at a zero angle (ΔI_0), which is approximately proportional to the micellar $M_{w,app}$: an initial steep increase in these two parameters leveled off to the constant value beyond GR of approximate 4. Notably, as depicted in Fig. 2, the size distribution was still unimodale for these micelles even after the crosslinking event, indicating that crosslinking induces essentially no variations in micellar polydispersity. Since, there were subtle changes in micellar d_c, ΔI_0, and PDI at GR > 50 (data not shown), only the micelles with GR < 50 will be used in the following experiments.

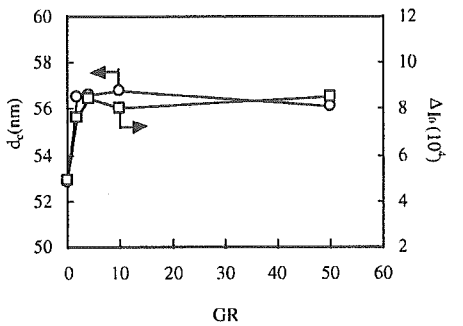

Fig. 1. Variations in d_c (○) and ΔI_0 (□) with increasing GR values obtained from DLS and SLS measurements for PEG–P(Asp)–NH_2/lysozyme micelles. Total concentration for each micelle system = 0.5 mg/mL; temperature = 25 ± 0.1 °C.

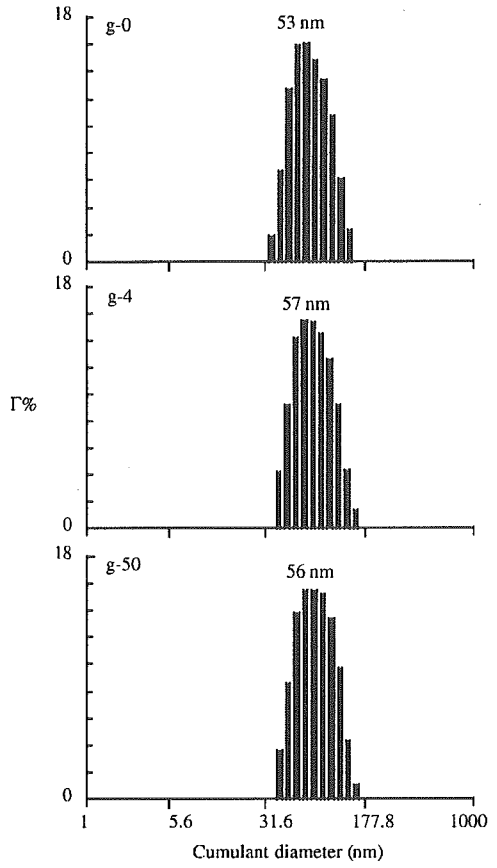

Fig. 2. Size distribution for g-0, g-4, and g-50 micelles, respectively. Total concentration for each micelle system = 0.5 mg/mL; temperature = 25 ± 0.1 °C.

3.2. Micellar stability versus ionic strength increase

Strong sensitivity to ionic strength is a well-known characteristic of polyion complexes due to the electrostatic shielding effect of salt that weakens the interactions between counter ions [12]. The crosslinking effect on the micellar stability against salt addition was estimated by comparing the changes in ΔI_0 and d_c with increasing NaCl concentrations for the micelles (1.0 mg/mL) with GR = 0, 2, 4, 10, 20, and 30, respectively.

The result in Fig. 3(a) (◆) shows monotonously decreased ΔI_0 values for un-crosslinked micelles (g-0), characteristic of micellar disintegration due to the decreased association force. d_c of g-0 micelles exclusively increased up to NaCl = 0.05 M (data not shown), and then became undetectable at NaCl > 0.05 M since increased NaCl concentration resulted in a drastically decreased photon count preventing the determination of the diffusion constant. Both of these results reflect the instability of g-0 micelles against salt addition. On the other hand, only a slight decrease in ΔI_0 and d_c values were observed for g-2 (▲) and g-4 (■) micelles, and at GR ≥ 10 (□, ○, △), both of these values reached a plateau until NaCl = 0.2 M (Fig. 3(a) and

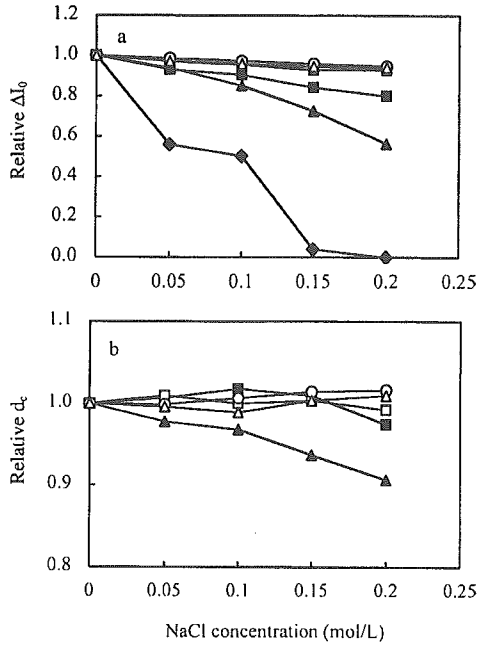

Fig. 3. Normalized variations in (a) ΔI_0 and (b) d_c values with increasing NaCl concentrations for g-0 (◆), g-2 (▲), g-4 (■), g-10 (□), g-20 (○), and g-30 (△) micelles, respectively. Total concentration for each micelle system = 0.5 mg/mL; temperature = 25 ± 0.1 °C.

(b)), indicating an improved micellar stability versus ionic strength due to the core crosslinking. Therefore, there exists a critical crosslinking degree over which PEG–P(Asp)–NH_2 block copolymers and lysozyme are fixed together physically and/or chemically due to the crosslinking event, which leads to an enhanced micellar stability against NaCl addition.

3.3. Importance of the ω-end amino groups in P(Asp) segments for micellar stabilization

In the case of PEG–P(Asp)–NH_2/lysozyme system, it is also possible that the ω-end amino groups in the P(Asp) segments may react with the glutaraldehyde. Thus, the contribution of these ω-end amino groups to the micellar stability was evaluated by comparing the micellar NaCl-stability for g-10 and g-10($COCH_3$) micelles, which were, respectively, formed from the PEG–P(Asp)–NH_2 and PEG–P(Asp)–NH–$COCH_3$ block copolymers. Worth noting, the g-10 and g-10($COCH_3$) micelles showed similar d_c and ΔI_0 values both before and after crosslinking at NaCl = 0 M (data not shown), emphasizing that the ω-end acetylation in the PEG–P(Asp)–NH–$COCH_3$ block copolymer had a negligible effect on the size and polydispersity of the micelles compared to g-10 micelles.

The NaCl-stability for g-10($COCH_3$) micelles was investigated using the same approach as in part 2, the result of which is shown in Fig. 4. At NaCl = 0.2 M, the ΔI_0 and d_c values both increased with time, and eventually precipitate

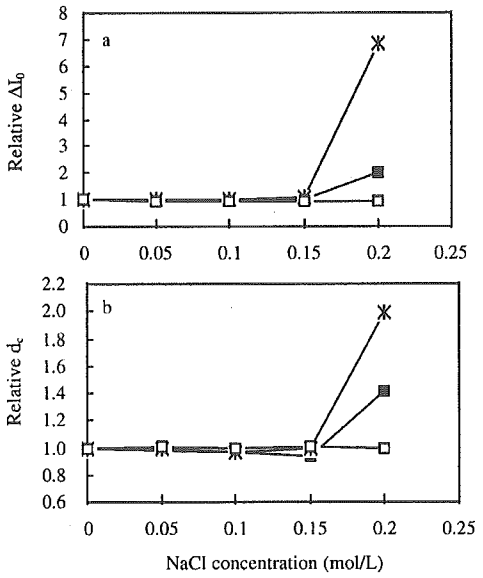

Fig. 4. Relative relationships of ΔI_0 and d_c with increasing NaCl concentrations for g-10 (□: 48 h) and g-10(COCH3) micelles (■: 24 h; ★: 48 h), respectively. Total concentration for each micelle system = 0.5 mg/mL; temperature = 25 ± 0.1 °C.

appeared in the g-10($COCH_3$) system (★ and ■; Fig. 4). These characteristics were obviously different from those of g-10 micelles, which showed constant ΔI_0 and d_c values at NaCl = 0.2 M even after 2 days (□; Fig. 4), indicating a decreased NaCl-stability for g-10($COCH_3$) micelles. In addition, in the UV absorption spectrum (Fig. 5) of the supernatant for g-10($COCH_3$) systems after formation of precipitate at NaCl = 0.3 M, the specific absorption around 280 nm for lysozyme could not be observed, consistent with the absence of lysozyme in the supernatant. Furthermore, ^1H NMR measurement revealed the existence of PEG–P(Asp)–NH–$COCH_3$ block copolymers in the supernatant (data not shown). Based on these UV and ^1H NMR results, it is reasonable to conclude that the PEG–P(Asp)–NH–$COCH_3$ block copolymers escaped from the g-10($COCH_3$) micelles

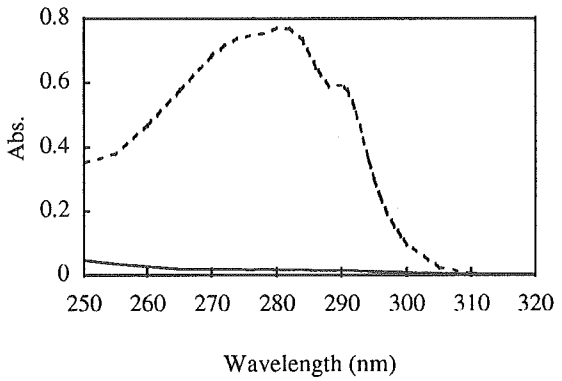

Fig. 5. UV absorption spectra for free lysozyme (0.3 mg/mL; broken line) and the supernatant from g-10(COCH3) system (solid line) at 0.3 M NaCl. Temperature = 25 °C.

at high salt concentration. Such event results from the diminished micellar association force and the absence of covalent bonding between the polymer and the lysozyme via glutaraldehyde bridges. Solubility of the system decreased as PEG–P(Asp)–NH–$COCH_3$ escaped into solution, and eventually, the crosslinked lysozyme precipitated. Hence, the ω-end amino groups in PEG–P(Asp)–NH_2 block copolymers, which may react with the glutaraldehyde, are indeed necessary to promote a better stability of crosslinked micelles against NaCl increase.

3.4. Extent of crosslinking reaction

Since, TNBS only reacts with free amino groups [10c], the lysine residues involved in the crosslinking reaction on the surface of lysozyme can be estimated by subtracting the TNBS reactable ones from the total lysine residues. As described above, the ω-end amino groups in P(Asp) segments may also react with TNBS. Nevertheless, they are in a magnitude around 12-fold less than the lysine residues, and it may be acceptable to assume that essentially the lysine residues in lysozyme are estimated by this analysis method. A suitable reaction time was decided by evaluating the time dependence of N_{lysine} (= number of free amino groups per lysozyme molecule) for the reaction of free lysozyme with TNBS. N_{lysine} did not significantly vary over 72 h. Reasonably, 100 h was chosen as a suitable reaction time for free lysozyme and g-0 micelles, because of no crosslinked lysine residues in them, and 72 h for crosslinked micelles.

The calculated results are summarized in Table 1. N_{lysine} was found to be about 6 for both the free lysozyme and entrapped-lyzozyme in g-0 micelles. In other words, all the lysine residues on the surface of free [13] as well as micelle-entrapped lysozymes can react with the TNBS, clearly showing the suitability of this analysis method to the PIC micelles. In the case of crosslinked micelles, $N_{lysine} \approx 2.6$, 1.8, 1.6, and 1.2 were separately calculated for g-4, g-10, g-20, and g-30 micelles, respectively, indicating that a higher crosslinking degree is achieved at a higher GR ratio. Combined with the NaCl-stability results, $N_{lysine} \approx 2$ seems to be the critical value, below which crosslinked micelles may become stable even at NaCl = 0.15 M.

3.5. Micellar spectroscopic characteristics

Spectroscopic properties for g-20 micelles were studied in order to examine the possible conformational changes of entrapped lysozyme due to the crosslinking reaction. As seen in Fig. 6(a), the CD spectrum of g-20 micelles in the short wavelength region (200–240 nm), indicative of lysozyme secondary structure, was superimposed on those of g-0 micelles and free lysozyme. In the long wavelength region (260–310 nm) characteristic of the environments of aromatic side chains in lysozyme (Fig. 6(b)), both of the CD spectra for g-20 and g-0 micelles were similar in shape to

Table 1
Number of un-crosslinked lysine residues per lysozyme molecule (N_{lysine}) determined by TNBS analysis

	Lysozyme	g-0 Micelle	g-4 Micelle	g-10 Micelle	g-20 Micelle	g-30 Micelle
N_{lysine}	5.9	6.1	2.6	1.8	1.6	1.2

the one of free lysozyme, but [θ] decreased in the order of free lysozyme > g-0 > g-20 micelles. These CD measurements suggest that in g-20 micelles, the secondary structure of lysozyme remains unchanged but the tryptophane (Trp) residues experience a different local environment.

The UV absorption spectrum of g-20 micelles showed a blue shift in the absorption maximum wavelength (λ_{max}) from 280 nm to around 274 nm (Fig. 7(a)). There was also a marked increase in the absorbance over the whole spectrum for both of the g-20 and g-0 micelles compared with free lysozyme, pointing out some changes in the local environment of Trp residues that possibly result from the micellization and the core-crosslinking events.

Furthermore, the fluorescence emission spectrum of g-20 micelles upon excitation at 293 nm was appreciably blue-shifted in the maximum emission wavelength (338.8 nm) compared to the fluorescence emission of free lysozyme (343.0 nm) and g-0 micelles (340.8 nm) (Fig. 7(b)), which suggests that the crosslinking may generate a less polar environment around the Trp residues [14]. Simultaneously, a 75% decrease in the fluorescence emission intensity was observed for the g-20 micelles compared with the free lysozyme, but only a slight decrease in the g-0 micelles, which indicates that the fluorescence emission intensity of g-20 micelles was quenched. Notably, all these observed spectroscopic characteristics for g-20 micelles agreed well with those previously reported for glutaraldehyde-crosslinked proteins, e.g. glucoamylase [15]. However, the molecular mechanisms responsible for such properties are still unclear because of the complicated reaction mechanisms for glutaraldehyde [16a] and thus unpredictable reaction products [16b,c]. One of the possible products in proteins crosslinked by glutaraldehyde can contain the quaternary pyridinium structure [17] shown in Scheme 1. Pyridinium analogues may have λ_{max} = 266 nm (1,3,4,5-substitution) or 276 nm (1,2,3,5-substitution) [18] close to that observed for the g-20 micelles (274 nm). Additionally, it is known that this pyridinium moiety effectively quenches the fluorescence emission of aromatic groups probably by an electron transfer mechanism [19]. It should be noted that recent studies have shown that the pyridinium moiety could effectively quench the fluorescence emission of Trp residues in proteins and the fluorescence emission maximum was then also blue-shifted [20]. Hence, this type of pyridinium

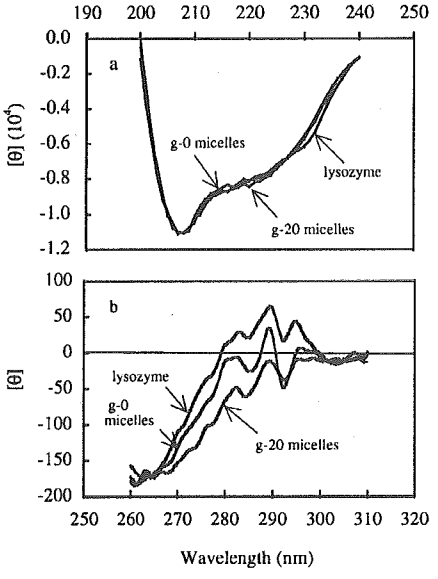

Fig. 6. CD spectra for free lysozyme, g-0, and g-20 micelles, respectively, (a) lysozyme = 0.2 mg/mL (lysozyme = 0.4 mg/mL for g-0 micelle system, total concentration of which was higher than cac); (b) lysozyme = 2.0 mg/mL; temperature = 25 °C.

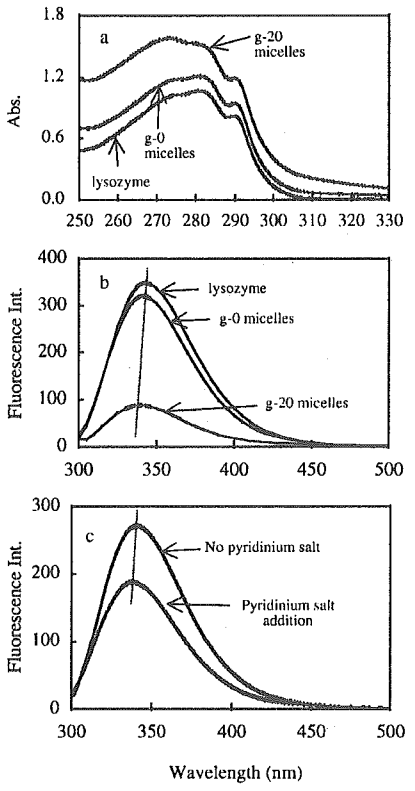

Fig. 7. Both of the UV absorption spectra; (a, lysozyme = 2.0 mg/mL) and fluorescence emission spectra; (b, lysozyme = 0.5 mg/mL) for free lysozyme, g-0, and g-20 micelles, respectively. And c is the fluorescence emission spectra (lysozyme = 0.5 mg/mL) for g-0 micelle before and after pyridinium salt addition. Temperature = 25 °C.

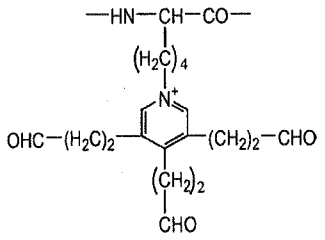

Scheme 1.

structures may also form in the crosslinked PIC micelles. Concrete evidence was obtained upon addition of a 500-fold excess of pyridinium chloride per lysozyme molecule to the g-0 micelles solution (lysozyme concentration = 0.5 mg/mL). Note that no significant micellar dissociation occurred at this salt concentration. The fluorescence spectrum measured after 24 h incubation at 25 °C is shown in Fig. 7(c). Obviously, a blue shift of the fluorescence emission wavelength maximum as well as a quenched fluorescence emission were observed for the g-0 micelles after pyridinium salt addition, which consistently support the pyridinium structure formation in the crosslinked micelles.

3.6. Critical association concentration (cac) for crosslinked PIC micelles

It has been reported that the critical association concentration (cac) of micelles might be calculated from the Debye plot of SLS (Eq. (5), a $KC/\Delta R_0$ curve against C) [8a,b]. However, for the core-crosslinked micelles, the dn/dc value, which is necessary to determine the K parameter, is not easily obtained by the method described previously [8a], because the amount of residual glutaraldehyde inside micellar core after dialysis is unknown. Hence, $C/\Delta I_0$ values, which are proportional to the $KC/\Delta R_0$ ones, were alternatively used and the respective $C/\Delta I_0$ curves plotted against C for g-0, g-10, and g-20 micelles obtained as demonstrated in Fig. 8, where all the $C/\Delta I_0$ values at 1 mg/mL were set to unity as controls. For g-0 micelles, the $C/\Delta I_0$ values increased with dilution due to the progressive decrease of the ΔI_0 values, indicative of micellar dissociation.

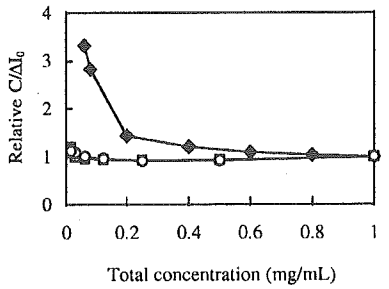

Fig. 8. Relative relationships of $C/\Delta I_0$ values with total concentration for each micelle system obtained from SLS measurements for g-0 (◆), g-10 (□), and g-20 (○) micelles, respectively. Temperature = 25 ± 0.1 °C.

Apparently, a different tendency was observed for the crosslinked micelles (g-10 and g-20), in which no significant increase in $C/\Delta I_0$ values appeared during dilution, suggesting that the cac value for crosslinked micelles is too low to be determined by the SLS measurements. Consequently, dilution stability of the crosslinked micelles was dramatically improved only by the crosslinking of micellar core.

3.7. Micellar pH-sensitivity

Micellar pH-sensitivity was also examined by the DLS and SLS measurements for g-0 (lysozyme concentration = 1.0 mg/mL) and g-20 (lysozyme concentration = 0.5 mg/mL) micelles at various pH values, which were separately prepared by 0.1 M HCl or NaOH addition to avoid significant deviations in the micellar concentration and the ionic strength of medium. Fig. 9 shows the pH dependence of d_c (Fig. 9(a)) and ΔI_0 (Fig. 9(b)) values for these two micelles. For an easy comparison, all the d_c and ΔI_0 values at pH = 7.4 were made to be unity as controls. As seen in Fig. 9(a), the d_c for g-0 micelles (◆) slightly decreased with decreasing pH values down to pH = 4.0, and then sharply increased to become five times higher than that at pH = 7.4. Conversely, with increasing pH values from 7.4, a notable increase in d_c was observed at pH > 10.5, close to the isoelectric point of lysozyme (= 11) [8a]. As seen in Fig. 9(b), similar but more remarkable variations in the ΔI_0 for g-0 micelles (◆) were observed, along with a steep decrease in ΔI_0 at pH > 10.5 and pH < 3.5. Both of the d_c and ΔI_0 results confirm the instability of g-0 micelles in acidic and basic environments, possibly as a result of the attenuated electrostatic interactions between the P(Asp) segments in block copolymer and lysozyme, due to the progressive protonation of COO^- groups in the P(Asp)

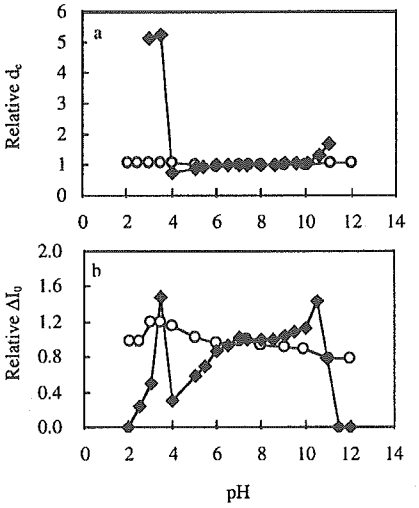

Fig. 9. Normalized variations in d_c (a) and ΔI_0 (b) with pH values, respectively, for g-0 (◆; 1.0 mg/mL) and g-10 micelles (○;0.5 mg/mL). Temperature = 25 ± 0.1 °C.

segments at pH<7.4 [21], and the deprotonation of NH_4^+ groups of the lysine residues in lysozyme at pH>7.4 [22]. At pH>10.5 and pH<3.5, the g-0 micelles dissociated because of the diminished association force.

On the other hand, for g-20 micelles, the fluctuations in d_c and ΔI_0 values (○) were obviously subtle compared with the g-0 micelles, suggesting that the crosslinking in the core substantially contributed to preserve the micellar structure even in conditions generated weak electrostatic interactions. Also, the resistance of g-20 micelles against pH decrease suggests that no azomethine bonds were formed in the crosslinking reaction of glutaraldehyde as such connectivity readily dissociates in acidic environment [23].

3.8. Micellar stability in the presence of organic solvents

Generally, proteins are instable in organic solvents because of destruction of their peculiar conformation [24]. To thoroughly estimate the properties of the crosslinked micelles, their tolerance against organic solvents addition was also evaluated. Hamaguchi et al. have shown the effects of dioxane addition on the thermal denaturing temperature of lysozyme (T_m) [25]. The T_m linearly decreased with an increase in dioxane volume, and down to 40 °C with 40 v/v% of dioxane, from which the T_m might be predicted down to around 30 °C with 60 v/v% of dioxane. To determine the dioxane volume that may denature lysozyme at 25 °C, turbidity measurements were undertaken for lysozyme solutions with different volumes of dioxane. A constant and an exclusively increased turbidity, respectively, corresponded to 40 and 50 v/v% of the dioxane within 30 min, showing that the lysozyme immediately denatured and precipitated in 50 v/v% of dioxane at 25 °C. According to this result, both of 50 and 60 v/v% of dioxane were separately added into g-0 and g-20 micelle solutions, and incubated in water bath at 25 °C over 24 h before DLS analysis, the results of which are summarized in Fig. 10 (g-0 micelle) and Fig. 11 (g-20 micelle), respectively. Notably, d_c increased for g-0 micelles after dioxane addition from 53 nm (dioxane content: 0 v/v%) to 451 nm (dioxane content: 50 v/v%) and 608 nm (dioxane content: 60 v/v%) (Fig. 10). Concomitantly, the size distribution became bimodal. In Fig. 11, although the d_c for g-20 micelles with 50 v/v% (51 nm) and 60 v/v% (50 nm) of dioxane slightly decreased from that in buffer only (56 nm), a unimodal size distribution was still present. Additionally, after removal of the added dioxane by dialysis against PBS solution, the d_c for g-20 micelles was recovered to the original value of 57 nm (50 v/v% dioxane→0 v/v% dioxane) and 59 nm (60 v/v% dioxane→0 v/v% dioxane). It is likely that the subtly decreased d_c for g-20 micelles upon dioxane addition may reflect a slight shrinking of PEG shell due to the decreased compatibility with dioxane [26], and/or the viscosity effect on the R_h (Eq. (4)) since dioxane has a higher viscosity index than water [27]. Consequently, crosslinking micellar core may improve the micellar

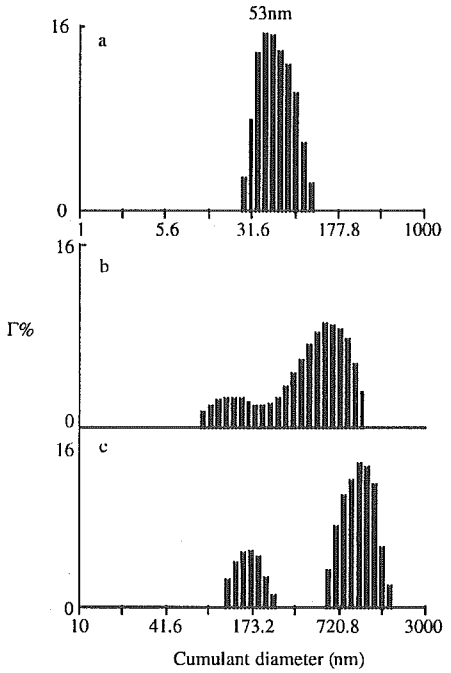

Fig. 10. Size distribution obtained from DLS measurements for g-0 micelles at 0 v/v% (a, total concentration=1.0 mg/mL, PDI=0.083), 50 v/v% (b, total concentration=0.5 mg/mL, PDI=0.244), and 60 v/v% (c, total concentration=0.4 mg/mL, PDI=0.278) of dioxane, respectively. Temperature=25±0.1 °C.

stability against dioxane addition, therefore, inhibiting lysozyme denature that might occur for un-crosslinked micelles with 50 or 60 v/v% of dioxane.

3.9. Apparent enzymatic activity

To specify the lysozyme activity within crosslinked PIC micelles, a synthesized substrate NP-$(GlcNAc)_4$ was employed and considering its small size, it can favorably diffuse into the micellar core, where it can be hydrolyzed [8c]. Here, only the apparent reactive velocity, v_{app}, calculated from the released amount of *p*-nitrophenol was evaluated, and more detailed information will be supplied elsewhere.

Fig. 12 shows the relative v_{app} values, respectively, for g-0, g-4, g-20 micelles and the v_{app} for free lysozyme set as unity. Obviously, the v_{app} values for both of the crosslinked and un-crosslinked micelles were around 2.5 times higher in magnitude than that for free lysozyme, suggesting that micellization facilitates the apparent lysozyme activity, and that core-crosslinking does not inhibit the enzymatic activity of the entrapped lysozyme at this NP-$(GlcNAc)_4$ concentration. The reason for this has been explained in our recent reports [8d,e]: PEG shell around the micelles favors substrate accumulation in micellar core, thus the substrate concentration in the core is higher than that around the micelles.

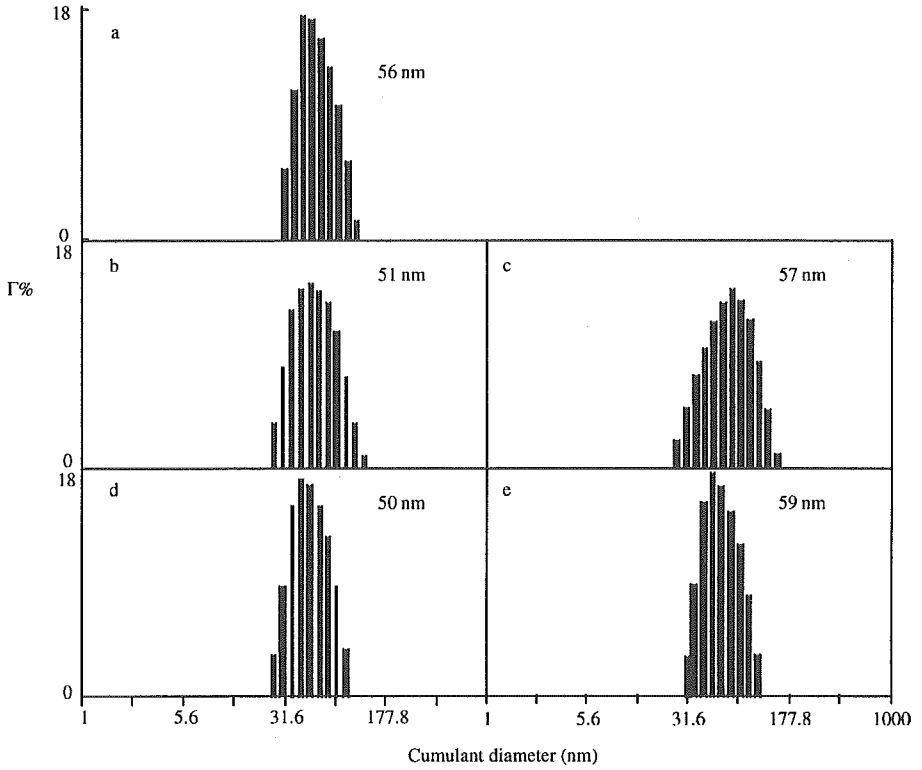

Fig. 11. Size distribution obtained from DLS measurements for g-20 micelles at 0 v/v% (a, total concentration = 0.5 mg/mL, PDI = 0.061), 50 v/v% (b: before dialysis, total concentration = 1.0 mg/mL, PDI = 0.046; c: after dialysis, total concentration was unknown because of significant variations in volume, PDI = 0.059), and 60 v/v% (d: before dialysis, total concentration = 0.8 mg/mL, PDI = 0.072; e: after dialysis, total concentration was unknown because of significant variations in volume, PDI = 0.068) of dioxane, respectively. Temperature = 25 ± 0.1 °C.

4. Conclusions

Simple glutaraldehyde addition to PEG–P(Asp)–NH_2/lysozyme micelles led to a successful crosslinking of the micellar core with insignificant changes in the micellar size and size distribution. Notably, both of the ω-end amino groups in PEG–P(Asp)–NH_2 block copolymers and lysine residues on the surface of lysozyme participated in the reaction with glutaraldehyde, resulting in a tightly fixed micellar core-shell structure responsible for the enhanced micellar stability not only towards dilution and ionic strength increase, but also dioxane addition and pH variation. A critical crosslinking degree for micelle stabilization requires an average reaction of 4 out of the 6-lysine residues with glutaraldehyde in each lysozyme molecule. Pyridinium analogues are expected to form in the crosslinking reaction between glutaraldehyde and the amino groups, as suggested by the blue shifted λ_{max} and quenched fluorescence emission for crosslinked micelles. More interestingly, the crosslinking of the micellar core has no significant interference with the apparent lysozyme activity in the micelles, keeping it even higher than that for free lysozyme.

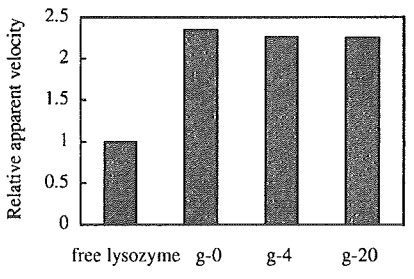

Fig. 12. Relative apparent reactive velocities, respectively, for free lysozyme, g-0, g-4, and g-20 micelles with identical lysozyme concentration (2.0 mg/mL) calculated from the released amount of *p*-nitrophenol at 400 nm. Temperature = 25 °C.

Acknowledgements

This work was supported by a Grant-in-Aid for Scientific Research from the Ministry of Education, Culture, Sports, Science and Technology (MEXT), Core Research for Evolution of Science and Technology (CREST), Japan Science and Technology Corporation (JST), and 21st century COE program 'Human-Friendly Materials based on Chemistry' from MEXT.

References

[1] (a) Merrifield BR. J Am Soc 1963;85:2149–54.
(b) Merrifield B. In: Fields GB, editor. Methods in enzymology, vol. 289, 1997. p. 3–13.
[2] Miller WL. Adv Exp Med Biol 1979;118:153–74.
[3] Wang W. Int J Pharm 1999;185:129–88.
[4] (a) Cohen S, Yoshioka T, Lucarelli M, Hwang LH, Langer R. Pharm Res 1991;8:713–20.
(b) Cleland JL, Jones AJS. Pharm Res 1996;13:1464–75.
(c) Schwendeman SP, Tobio M, Joworowicz M, Alonso MJ, Langer R. J Microencapsulation 1998;15:299–318.
(d) Lam XM, Duenas ET, Cleland JL. J Pharm Sci 2001;90:1356–65.
[5] (a) Prestrelski SJ, Tedishi N, Arakawa T, Carpenter JF. Biophys J 1993;65:661–71.
(b) Costantino HR, Langer R, Klibanov AM. Pharm Res 1994;11: 21–9.
(c) Costantino HR, Langer R, Klibanov AM. J Pharm Sci 1994;83: 1662–9.
(d) Dong A, Prestrelski SJ, Allison SD, Carpenter JF. J Pharm Sci 1995;84:415–24.
(e) Sah H. J Pharm Sci 1999;88:1320–5.
(f) Sah H. PDA J Pharm Sci Technol 1999;53:3–10.
(g) Vande Weert M, Hoechstetter J, Hennink WE, Crommelin DJ. J Controlled Release 2001;68:351–9.
[6] Jaturanpinyo M, Harada A, Yuan X-F, Kataoka K. Bioconjugate Chem 2004;15:344–8.
[7] (a) Margel S, Rembaum A. Macromolecules 1980;13:19–25.
(b) Damink LHHO, Dijkstra PJ, Van Luyn MJA, Van Wachem PB, Nieuwenhuis P, Feijen J. J Mater Sci 1995;6:460–72.
[8] (a) Harada A, Kataoka K. Macromolecules 1998;31:288–94.
(b) Harada A, Kataoka K. Langmuir 1999;15:4208–12.
(c) Harada A, Kataoka K. J Am Chem Soc 1999;121:9241–2.
(d) Harada A, Kataoka K. J Controlled Release 2001;72:85–91.
(e) Harada A, Kataoka K. J Am Chem Soc 2003;125:15306–7.
[9] (a) Yokoyama M, Inoue S, Kataoka K, Yui N, Sakurai Y. Makromol Chem Rapid Commun 1987;8:431–5.
(b) Yokoyama M, Inoue S, Kataoka K, Yui N, Okano T, Sakurai Y. Makromol Chem 1989;190:2041–54.
[10] (a) Habeeb AFSA. Anal Biochem 1966;14:328–36.
(b) Freedman BR, Radda GK. Biochem J 1968;108:383–91.
(c) Satake K, Okuyama T, Ohash M, Shinoda T. J Biochem (Tokyo) 1960;47:654–60.
[11] Gulari E, Tsunashima Y, Chu B. J Chem Phys 1979;70:3965–72.
[12] (a) Abe K, Ohno H, Tsuchida E. Makromol Chem 1977;178: 2285–93.
(b) Tuchida E, Osada Y, Ohno H. J Macromol Sci Phys B 1980;17: 683–91.
[13] Blake CCF, Mair GA, North ACT, Phillips DC, Sarma VR. Proc R Soc Ser B 1967;167:365–77.
[14] (a) Nishimoto E, Yamashita S, Yamasaki N, Imoto T. Biosci Biotech Biochem 1999;63:329–36.
(b) Van Duuren BL. J Org Chem 1961;26:2954–60.
[15] Takahashi T, Hirata N, Hamada M, Irie M. Chem Pharm Bull 1986; 34:798–805.
[16] (a) Hermanson GT, editor. Bioconjugate techniques.
(b) Habeeb AFSA, Hiramoto R. Arch Biochem Biophys 1968;126: 16–26.
(c) Nakagawa T, Izawa K, Yagi S, Shibukawa A, Tanaka H, Tashima T, et al. Chem Phys Bull 1989;37:2463–6.
[17] Hardy PM, Nicholls AC, Rydon HN. J Chem Soc Perkin Trans 1 1976;9:958–62.
[18] Elsden TDF, Partridge SM. Nature 1963;200:651–2.
[19] (a) Davis GA. J Chem Soc Chem Commun 1973;19:728–9.
(b) Hann RA, Rosseinsky DR, White TP. J Chem Soc Faraday Trans II 1974;9:1522–5.
[20] (a) Sepcic K, Poklar N, Vesnaver G, Fournier D, Turk T, Macek P. J Protein Chem 1999;18:251–7.
(b) Diaz X, Abuin E, Lissi E. J Photochem Photobiol A 2003;155: 157–62.
[21] Harada A, Kataoka K. Macromolecules 1995;28:5294–9.
[22] (a) Tanford C, Wager ML. J Am Chem Soc 1954;76:3331–6.
(b) Sakakibara R, Hamaguchk K. J Biochem 1968;64:613–8.
(c) Bradbury JH, Brown LR. Eur J Biochem 1973;40:565–76.
[23] Prankerd RJ, Stella VJ. Int J Pharm 1989;52:71–8.
[24] Sah H. J Controlled Release 1999;58:143–51.
[25] (a) Hamaguchi K, Kurono A. J Biochem 1963;54:497–505.
(b) Hamaguchi K, Sakai H. J Biochem 1965;57:721–32.
[26] Monique G. Polymer 1983;24:865–70.
[27] Marsh KN. Pure Appl Chem 1980;52:2393.

Multifunctional polymeric micelles with folate-mediated cancer cell targeting and pH-triggered drug releasing properties for active intracellular drug delivery†

Younsoo Bae,[a] Woo-Dong Jang,[a] Nobuhiro Nishiyama,[b] Shigeto Fukushima[a] and Kazunori Kataoka*[ab]

Received 7th January 2005, Accepted 17th June 2005
First published as an Advance Article on the web 30th June 2005
DOI: 10.1039/b500266d

A new type of multifunctional polymeric micelle drug carrier for active intracellular drug delivery was prepared and characterized in this study. The micelle is a nano-supramolecular assembly with a spherical core–shell structure, and its surface and core were modified with piloting molecules for cancer cells and pH-sensitive drug binding linkers for controlled drug release, respectively. In order to prepare such micelles, self-assembling amphiphilic block copolymers, folate–poly(ethylene glycol)–poly(aspartate hydrazone adriamycin) [Fol–PEG–P(Asp-Hyd-ADR)], were specially designed and synthesized by installing a molecular promoter to enhance intracellular transport, folate (Fol), at the end of the shell-forming PEG chain and conjugating the anticancer drug, adriamycin (ADR), to the side chain of the core-forming PAsp segment through an acid-sensitive hydrazone bond. Because folate-binding proteins (FBP) are selectively overexpressed on the cancer cell membranes, the folate-bound micelles (FMA) can be guided to the cancer cells in the body, and after the micelles enter the cells, hydrazone bonds are cleaved by the intracellular acidic environment (pH 5–6) so that the drug release profile of the micelles is controlled pH-dependently. In this regard, FBP-binding selectivity of the prepared FMA was evaluated by surface plasmon resonance (SPR) measurements. The tetrazolium dye method (MTT assay) using human pharyngeal cancer cells (KB cell) revealed that FMA significantly improved cell growth inhibitory activity in spite of a short exposure time due to the selective and strong interaction between folate molecules and their receptors. Subsequent flow cytometric analysis showed that cellular uptake of FMA significantly increased. Consequently, these findings would provide one of the most effective approaches for cancer treatment using intracellular environment-targeting supramolecular drug carriers.

Introduction

Biologically active materials for cancer chemotherapy are usually selected using cell biology and pharmacology, which provide a rationale for understanding the Absorption, Distribution, Metabolism and Excretion (ADME) of exogenous molecules in the body. A number of studies have claimed that polymer science and supramolecular chemistry can offer the most adequate and suitable means for designing functional nano-bio devices.[1–5] For these reasons, growing interest is currently focused on the creation of functional polymeric nano-carriers that regulate ADME of drugs at the boundary between biochemistry and nano-technology.[6,7]

Among such carriers, spherical supramolecular nano-assemblies from amphiphilic block copolymers, called polymeric micelles, have attracted considerable attention in the field of drug delivery systems due to their unique characteristics such as high water-solubility, high drug loading capacity and low toxicity, which are induced by the prolonged circulation in the blood and enhanced accumulation in tumor tissue.[8] In particular, the intracellular environment-sensitive polymeric micelle, that can release the loaded drug, adriamycin (ADR), through sensing pH decreases in the acidic endocytic compartments such as endosomes (pH 5–6) and lysosomes (pH 4–5), has recently been reported to minimize non-specific systemic spread of toxic drugs while maximizing tumor-directed drug delivery efficiency.[9,10] Indeed, animal studies have elucidated that this type of micelle significantly improves the bioavailability of existing drugs by controlling the drug release profile, inducing high antitumor activity with extremely low drug toxicity and avoiding clearance by the host defense system and uptake by normal tissue. Nevertheless, cell growth inhibitory activity still needs to be improved because the effective dose for cancer treatment using these micelles was relatively high, 4-fold compared with free drugs. However, *in vitro* activity of most polymer–drug conjugates is known to decrease as their biological behavior, that is involved with

[a]*Department of Materials Science and Engineering, Graduate School of Engineering, The University of Tokyo, 7-3-1 Hongo, Bunkyo-ku, Tokyo 113-8656, Japan. E-mail: kataoka@bmw.t.u-tokyo.ac.jp; Fax: +81-3-5841-7139; Tel: +81-3-5841-7138*
[b]*Center for Disease Biology and Investigative Medicine, Graduate School of Medicine, The University of Tokyo, 7-3-1 Hongo, Bunkyo-ku, Tokyo 113-0033, Japan*

† Electronic supplementary information (ESI) available: Quantitative introduction of hydrazide groups to the PBLA block and correlation between number of linkers and drug release profile of the micelle. See http://dx.doi.org/10.1039/b500266d

cellular uptake by an endocytotic pathway and relatively slow drug release, often works to the disadvantage of exerting drug efficacy compared to free drugs that rapidly move into the cell interior.[11] Consequently, it is expected that if the macromolecular drug carriers were actively transported inside the cells, the bioavailability of the carriers should increase more than the drug carrier system that simply exploits passive drug delivery. In order to achieve both these goals, the micelles are also required to selectively and strongly interact with targeted cells so that intracellular transport can be controllable. On the basis of this background, we have developed a new type of multifunctional polymeric micelle drug carrier system that will actively enhance its capability to deal with intracellular drug delivery to the targeted cancer cells (Fig. 1).

In the case of carriers for targeting cancer cells, the fundamental problems such as intracellular transport and the release of incorporated materials are often encountered during the materials' intracellular movement. These problems are particularly crucial to the carriers in terms of the delivery of materials that should become pharmaceutically effective after entering cells. To satisfy the former requirement, the micelles we present in this study are equipped with folate-ligands, which are non-immunogenic and stable during transportation *in vivo* without denaturation. For the latter requirement, the pH-sensitivity that enables selective drug release in intracellular acidic compartments, endosomes (pH 5–6), is used. Folate is a vitamin with low molecular weight (MW = 441.4) and behaves as a ligand because it has high affinity for its receptors (K_d < 1 nM), folate-binding proteins (FBP), that are selectively overexpressed on the surface of cancer cells.[12,13] Therefore, its conjugates with an appropriate design can be directed to the cancer cells in the body and internalized in the target cells *via* receptor-mediated endocytosis.[14–16] In the meantime, there is notable intracellular behavior of the folate-bound materials after ligand-mediated endocytosis, which distinguishes the folate ligand from other types of ligands such as antibodies, hormones and peptides. In contrast to the fact that most ligands are internalized and transported to the lysosomes, folate-conjugates remain in 'recycling endosomes (pH 5–6)' or escape into the cytoplasm, and such a characteristic plays a crucial role in accelerating intracellular uptake of the materials by the cell, avoiding the possible effects of lysosomal enzyme action.[17–19]

Therefore, the experimental results discussed in this study will present clear information about the effects of folate ligands on biological activity of the intracellular drug delivery when using the supramolecular drug carriers that are selectively activated in the cell.

Results and discussion

Design of the micelles and synthesis of their constituent bifunctional block copolymers

To prepare the folate-bound micelles, self-assembling amphiphilic block copolymers, folate–poly(ethylene glycol)–block–poly(aspartate hydrazone adriamycin) [Fol–PEG–p(Asp-Hyd-ADR) **11**], were designed and synthesized by developing a new and optimized synthetic protocol of both folate and poly(ethylene glycol) (PEG) to introduce functional groups for conjugation (Scheme 1). In general, two methods can be used to conjugate folate onto the surface of the polymeric micelles: (i) preparation of a surface-activated micelle followed by the conjugation of folate molecules by mixing them in the solution, and (ii) conjugation of folate molecules onto the constituent block copolymers followed by the preparation of the micelles with folate-bound block copolymers. The former may be a simple method to prepare the surface-modified micelles. However, it is unlikely to ensure

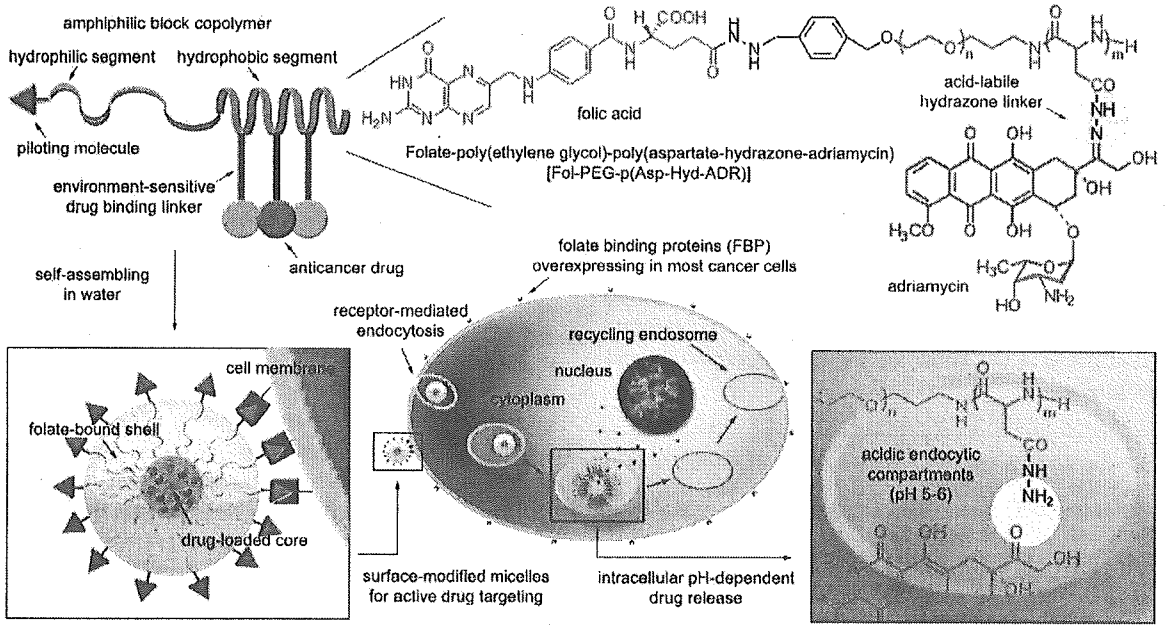

Fig. 1 Preparation of multifunctional polymeric micelles with tumor selectivity for active drug targeting and pH-sensitivity for intracellular site-specific drug transport. Folic acid with high-tumor affinity due to the overexpression of its receptors was conjugated onto the surface of the micelle.

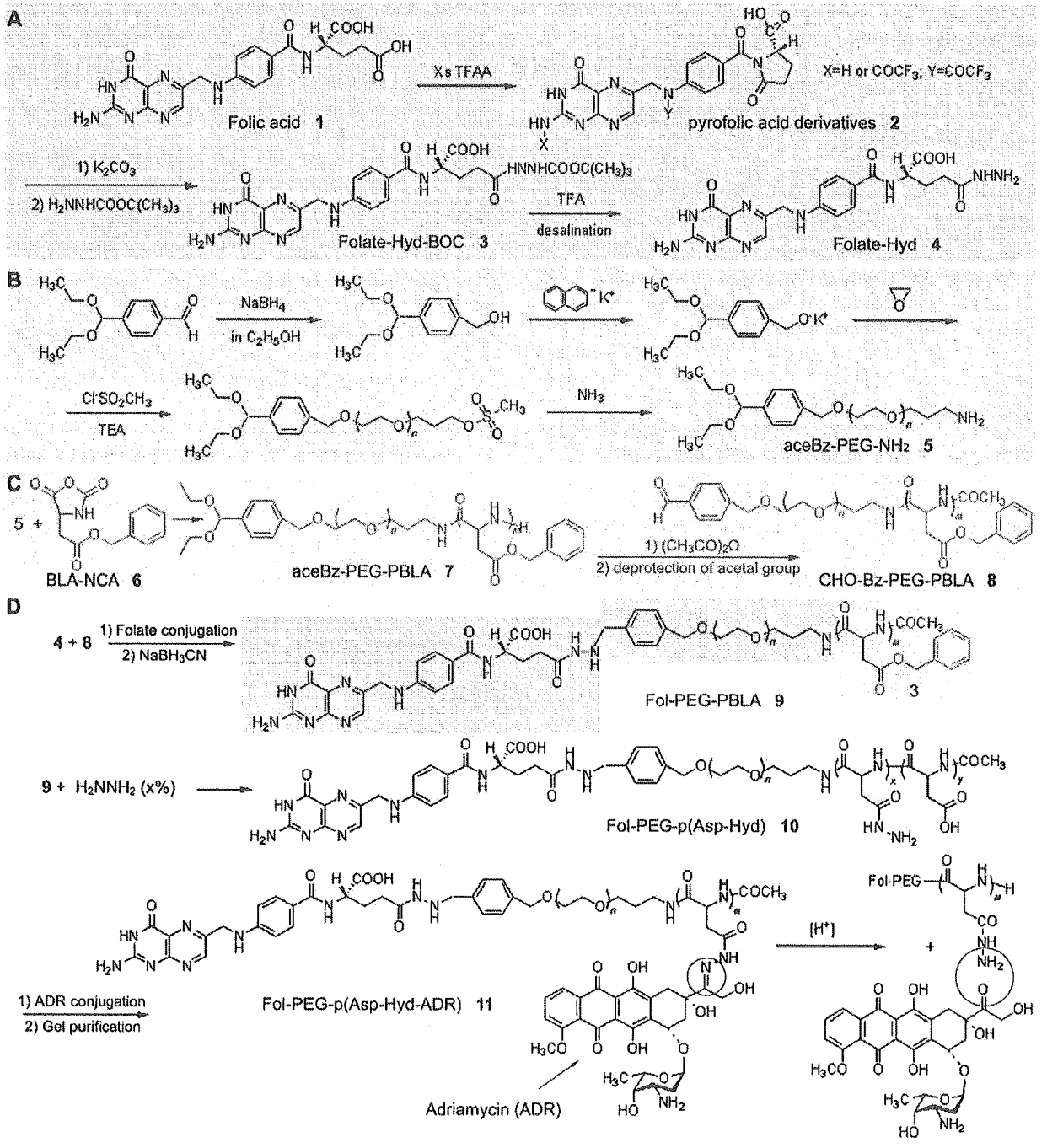

Scheme 1 Synthetic procedure of folate–poly(ethylene glycol)–poly(aspartate hydrazone adriamycin) block copolymers (D). Folate-hydrazide (A), α-4-(diethoxymethyl)benzyl-ω-amine-poly(ethylene glycol) (B), and aldehyde-benzyl-poly(ethylene glycol)-poly(β-benzyl L-aspartate) (C) were prepared prior to synthesis of the product.

high loading contents of folate molecules because the reaction rate is usually low and a cumbersome process of removing unreacted folate molecules is inevitably required. Moreover, the presence of unreacted ligand molecules, free folate, may hamper the binding between folate-bound micelles and folate-binding proteins (FBP) through competitive interaction. In contrast, the latter method, which was adopted in this study, requires a somewhat complex synthetic route involving the protection of functional groups to prevent side reactions, but has several advantages including quantitative reactions and characterization of the products. An impediment to the preparation of folate-conjugates, isomerization between inactive α-conjugates and active γ-conjugates, can be overcome, and this is quite crucial when preparing folate-conjugates. It has been reported that isomerization of folate-conjugated derivatives frequently occurs, in the case of DCC-coupling for

instance, and affects the FBP-binding selectivity of folic acid.[20] Therefore, the present synthetic route is probably one of the the best ways to conjugate folic acid as well as anticancer drugs with PEG at its γ-position to maintain FBP-binding activity and hydrazide groups at the drug-binding moiety of the side chain, respectively.

Synthesis of block copolymers and preparation of the folate-bound micelles

As described above, the micelles were prepared after the synthesis of folate–polymer conjugates to maintain FBP-binding activity. This is achieved by the design of an end-group functionalized folate and PEG.

Treatment of folic acid **1** (Fig. 2A) with an excess amount of trifluoroacetic anhydride in THF produces $N^{2,10}$-bis(trifluoroacetyl)-pyrofolic acid **2**.[21] By adding water, the compound affords N^{10}-(trifluoroacetyl)-pyrofolic acid and can be further transformed to pyrofolic acid *via* deacylation with K_2CO_3. However, both N^{10}-(trifluoroacetyl)-pyrofolic acid and pyrofolic acid are generally known as isomers, and the two imide carbonyl groups (γ-carbonyl and pteroic carbonyl) of pyrofolic acid derivatives, N^{10}-(trifluoroacetyl)-pyrofolic acid and pyrofolic acid, can react with nucleophiles. For these reasons, the products were purified to confirm the absence of pteroic acid derivatives by using a preparative HPLC and TLC, and pure folate–hydrazide–BOC (Fol–Hyd–BOC) **3** was successfully collected (Fig. 2B).

From the GPC analysis, the weight-average molecular weight (M_w) and the molecular weight distribution (M_w/M_n) of α-4-(diethoxymethyl)benzyl-ω-amine–poly(ethylene glycol) [aceBz–PEG-NH_2 **5**] were determined to be 10 159 and 1.02, respectively. The molecular weight was in accordance with the estimated value calculated from the ratio between monomers and initiators and its distribution was extremely narrow. These results indicate that the polymerization of EO proceeds without any side reactions by using potassium 4-(diethoxymethyl)benzylalkoxide (PDA) as an initiator.[22] The end-group was then checked by ^{1}H-NMR, comparing the peaks of PEG and 4-(diethoxymethyl)benzyl alcohol. The molecular weight was determined to be 10 971 from the peak intensity ratio of PEG (-OCH_2CH_2-) and benzylacetal [$(CH_3CH_2O)_2CH$-], which is in a good agreement with the M_w determined by GPC (10 159). Fig. 2C shows the ^{1}H-NMR peak of

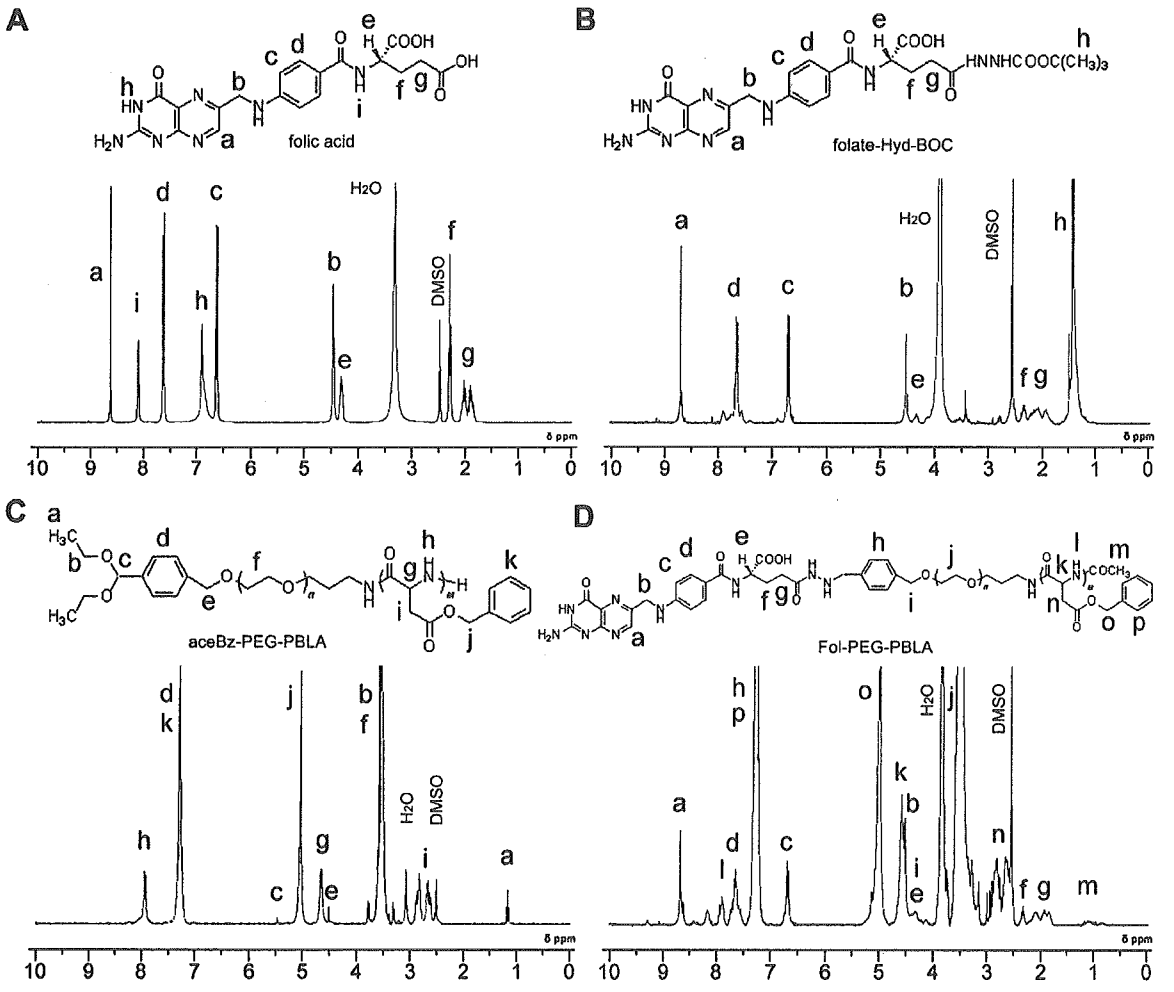

Fig. 2 ^{1}H-NMR spectra of folate (A), folate–hydrazide–BOC (B), 4-(diethoxymethyl)benzyl–poly(ethylene glycol)–poly(β-benzyl L-aspartate) (C) and folate–poly(ethylene glycol)–poly(β-benzyl L-aspartate) (D).

α-4-(diethoxymethyl)benzyl-poly(ethylene glycol)-poly(β-benzyl-L-aspartate) [aceBz–PEG–PBLA 7] synthesized *via* ring-opening polymerization of β-benzyl L-aspartate–*N*-carboxy-anhydride (BLA–NCA) by using **5** as a macromolecular initiator.

In the case of folate–poly(ethylene glycol)–poly(β-benzyl-L-aspartate) [Fol–PEG–PBLA **9**], the molecular weight and its distribution were 22 673 and 1.142 respectively which were determined by GPC equipped with a UV-VIS detector (360 nm) to confirm the conjugation between folate and PEG. ^{1}H-NMR also supported that the conjugation of folate to PEG was successfully carried out because a peak of aldehyde groups of unreacted PEG was not observed after the reaction (Fig. 2D). The anticancer drug, adriamycin (ADR), was introduced to Fol–PEG–PBLA block copolymers through an acid-sensitive hydrazone bond, and drug-loading contents and pH-sensitive drug release profiles of the folate-bound pH-sensitive micelle with ADR (FMA) were calculated by reversed phase liquid chromatography referring to a method reported elsewhere.[10] The compositions of **11** were 12–32–21, denoting that the polymer backbones consist of PEG with the molecular weight of 12 000 g mol^{-1} for the shell-forming segment, PBLA with 32 repeating units for the core-forming segment, and 21 hydrazide groups that are substituted for benzyl groups of PBLA for drug-binding. **11** formed spherical micelles with 63.4 nm diameters in aqueous solutions, which was confirmed by DLS. In the meantime, the folate-unbound pH-sensitive micelle with ADR (MA) was prepared from α-methoxy-poly(ethylene glycol)–poly(aspartate hydrazone adriamycin) [PEG–p(Asp-Hyd-ADR)] as control. The compositions of its constituent block copolymer PEG–p(Asp-Hyd-ADR) was 12–37–28, denoting that the polymer backbones consisted of PEG with molecular weight of 12 000 g mol^{-1}, PBLA with 37 repeating units, and 28 hydrazide groups substituted for benzyl groups of PBLA for drug-binding. The number of hydrazide groups for drug-binding was optimized by considering stability and the drug release profile of the micelles[9,10] (see also supporting information).† Prepared MA had 65 nm diameters, which were also determined by DLS. The size distribution of the micelles, expressed as polydispersity index (μ/Γ^2), was 0.155 and 0.168 for MA and FMA, respectively.

FBP-binding selectivity of the micelles

The FBP-binding effect of FMA was evaluated by surface plasmon resonance (SPR) measurements. For the experiments, FBP was immobilized onto a dextran-coated gold sensor chip, which was freshly prepared for each sample injection. The analysis showed that FMA not only effectively recognized but also strongly bound to the FBP (Fig. 3). Interestingly, once it binds, even though excess amounts of free folic acid (500 μg ml^{-1}) were added, FMA was not displaced or detached. On the other hand, when both FMA and free folic acid were injected at the same time, the FBP-binding effect of FMA obviously decreased. These results can be explained by the fact that FMA can bind FBP with a strong multivalent form, and binding sites are saturated and blocked in the presence of free folate molecules. Such characteristic behavior was not shown in the case of MA used as control. Therefore, it

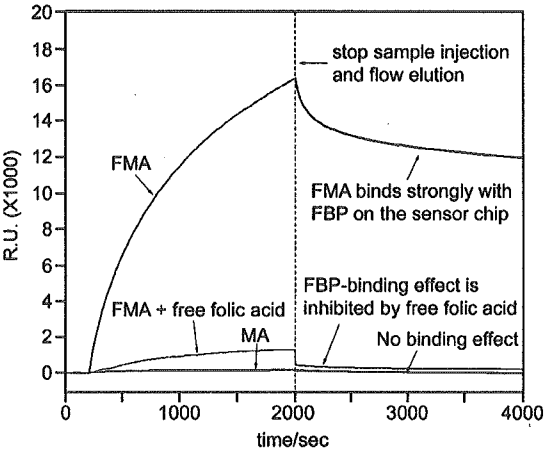

Fig. 3 Evaluation of FBP-binding selectivity of folate-bound micelles by using surface plasmon resonance (SPR) measurement (eluent: 100 mM phosphate buffer, pH 7.4; flow rate: 10 μl min^{-1}; density of folate-binding protein: 3 ng mm^{-2} per channel; sample concentration: 200 μg ml^{-1}).

is clearly revealed that FMA exhibits selective FBP-binding behavior, and the concept described in this research would be an effective approach for designing environment-sensitive polymeric micelle drug carriers for specific recognition of cancer cells in the body.

Evaluation of *in vitro* cytotoxic acitivity of FMA

SPR measurements showed that the FMA has strong and selective FBP-binding effects. Meanwhile, it is generally accepted that FBPs are overexpressed on the cell membranes of cancer cells.[23] Folate-bound carriers, therefore, are expected not only to increase the tumor-specific accumulation but also to reduce undesired distribution in normal tissues, reducing side effects from drug toxicity. In order to verify whether the FBP-binding effect of FMA is also active against living cells, *in vitro* growth-inhibition tests were carried out using human pharyngeal cancer cells (KB cell).

KB cells are widely used for evaluating the interaction between folate-mediated drug delivery systems and cancer cells due to their high affinity FBP-binding effect that has been studied and well elucidated by a large number of scientists over decades even though its contamination by HeLa cells is suspicious.[24,25] As described in the experimental section, KB cells were incubated with FMA, MA and free ADR, with exposure times of 3 h and 24 h. Post-incubation was carried out for 24 h after drug exposure, considering the fact that the cytotoxicity of the intracellular environment-sensitive drug carriers has a tendency to increase time-dependently accompanying drug release.[26–28] Fig. 4 shows that FMA enhances cell-growth inhibitory activity effectively, and we hypothesized it is probably due to the accelerated intracellular transport of the micelles by folate installation on their surfaces. Although both FMA and MA showed the delayed cytotoxicity changing with exposure time, only FMA showed effective growth-inhibitory activity with a short exposure time, clearly demonstrating that each micelle undergoes a different mechanism of